ORIGINAL RESEARCH

Eccentric steel brace retrofit for seismic upgrading of deficient reinforced concrete frames

Naveed Ahmad[1] **· Mostafa Masoudi**[2]

Abstract

The paper presents a simplified static force-based procedure for seismic retrofit design of RC frames using internal eccentric steel braces (ESBs), connected to long beam at distance of L/8 from beam ends, to enhance seismic resistance of the frame. The technique uses the linear static procedure given in ASCE 7-16 for calculation of appropriate design base shear for frame analysis, and the AISC 360-16 seismic provisions for preliminary design of steel braces. Response modification factor R was derived based on simplified kinematics of rigid frame response and flexure hinging of link beam, to reduce the elastic base shear force for lateral load analysis of frame and design of steel braces. This shifts plastic hinges from columns, and reduces joint shear deformation, by means of capacity protected braces and beam shear. The procedure was used for the preliminary design of ESB retrofitting technique for a two-story RC frame, employing hollow box steel sections. Quasi-static cyclic tests were performed on both as-built and ESB retrofitted portal frame panels under multiple-levels of lateral displacements demands. The tests performed on frames were analysed to understand the damage mechanism and retrieve the essential seismic response properties: force–displacement capacity curves, hysteretic cyclic response and hysteretic damping, and to establish performance-based story drift limits. The experimental data was used to calibrate finite element based nonlinear numerical models in SeismoStruct. Nonlinear static pushover analysis of considered two-story ESB retrofitted frame was carried to quantify structure ductility and response modification factors. The preliminary design was verified through nonlinear time history analysis (NLTHA) for both design base earthquakes and maximum considered earthquakes. Proposed seismic design of ESB retrofit for multi-stories RC frames having three to six stories has been presented and verified through NLTHA. It indicates the promising behaviour of ESB retrofit technique as well as the efficiency of the proposed simplified design procedure.

Keywords Eccentric steel braces · Seismic upgrade · Retrofitting · ASCE 7-16 · AISC 360-16

✉ Naveed Ahmad
  naveed.ahmad@uetpeshawar.edu.pk

1   Earthquake Engineering Center, UET Peshawar, Peshawar, KP, Pakistan

2   K. N. Toosi University of Technology, Tehran, Iran

1 Introduction

FEMA 547 (2006) has listed a number of common retrofitting techniques used for seismic upgrade of existing reinforced concrete (RC) frames. These included global retrofitting techniques e.g. adding reinforced masonry or concrete walls, steel braced frames, seismic isolation and supplemental energy dissipaters as well as member level retrofitting techniques like e.g. jacketing of columns and beams using concrete/steel or fiber composite wraps and strengthening of beam-column joints. However, the selection of any of the technique depends on various technical, financial and sociological considerations. The use of steel bracing system is preferred for seismic upgrade of RC frames due to its high strength to weight ratio, simplicity in application with minimal disruption, rapid construction and the ability to enhance global seismic resistance of structure. The steel braced frame can be attached to the existing structure from outside externally (Badoux and Jirsa 1990; Bush et al. 1991; Higashi et al. 1981; Nateghi-Alahi 1995) or internally within the RC frame panels (Chaulagain et al. 2015; Hjelmstad et al. 1988; Ohishi et al. 1988; Masri and Goel 1996; Tagawa et al. 1992; Usami et al. 1988). The promising behavior of internal bracing system that utilizes diagonal braces directly connected to the RC frame (Maheri and Sahebi 1997; Mahrenholtz et al. 2014), which has also eliminated the need for the intermediary steel frame, have prompted the use of direct internal steel braces for seismic rehabilitation of RC frame structures using concentric braces (Abou-Elfath and Ghobarah 2000) or eccentric braces (Ghobarah and Abou-Elfath 2001). Alternatively, a variety of dissipating and viscous dampers have been proposed as bracing system for existing structures to control deformation demands on structures subjected to seismic actions (Mazza and Vulcano 2015; Kim and Choi 2006; Lin et al. 2003; Rodrigues et al. 2012; Sorace et al. 2012; Mazza 2019).

Frame with concentric braces, where no eccentricity of connections exist, resist lateral loads through truss action in which diagonal braces are subjected to tension and compression (AISC 341-16 2016). The diagonal braces in both types of frames are subjected to large axial forces and minimum bending actions. Although initial stiffness of the concentric braced frame is higher, which is favorable for frame responding elastically to control vibration (e.g. winds and small-to-moderate earthquakes), inelastic deformability of concentric braced frame, which varies from 0.30 to 0.50% story drift (AISC 341-16 2016), is significantly lower than the code permitted story drift of 2.50%. As a consequence, concentric braced frame attracts higher inertial forces during extreme earthquake. The design of concentric braced frame permits braces to yield in tension and buckle inelastically in compression for dissipating seismic energy to reduce seismic demands, therefore, tensile yielding and compression buckling of diagonal braces as well as limited inelasticity in gusseted connections (Sen et al. 2019) characterize the response of concentric braced frame. However, this depends on the slenderness ratio of brace (Nakashima and Wakabayashi 1992; Shibata et al. 1973). The buckling of braces causes reduction in the lateral force–displacement hysteretic response of frame, termed as pinching, and can lead to soft-story mechanism in case the braces buckle in one story before those in the other stories. The AISC Seismic Provisions (AISC 341-16 2016) limit the brace slenderness to avoid such problems and to ensure stable hysteretic response of frame. Additionally, quality and detailing of bracing system components (brace, gusset plate, beam, column, welds, bolts) alters the yielding mechanism of concentric braced frame (Lehman et al. 2008). Past earthquakes have revealed the poor performance of concentric braces due to improper design and constructions, which have resulted in collapse of structures (Tremblay et al. 1995, 1996).

On the contrary, frame with eccentric braces, where eccentricity of connections is deliberately induced, respond to lateral loads through a mix of truss and flexure actions in system, therefore, this system combines the advantages of both the braces and frame (Roeder and Popov 1978). In case of an eccentric braced frame, each diagonal brace is connected to beam at some distance from the centerline of the beam. The segment of beam between the two diagonal braces or between brace and column is termed as link, which is subjected to high shear and bending forces. The system inelastic deformation capacity is provided by the flexure or shear deformation of link; however the yielding mechanism and deformation capacity of frame depends on the moment-to-shear ratio of link. The length of link governs the initial stiffness of frame i.e. frame with shorter links exhibit high initial stiffness (Hjelmstad and Popov 1984). The design ensures flexural yielding of link beam and elastic response of braces therefore the system exhibit high initial stiffness, stable hysteretic response and high deformation capacity. This type of frame has the additional advantage of accommodating door or window in the frame panel. Experimental studies have revealed that RC frames retrofitted with eccentric steel braces provide sufficient ductility to system in comparison to other bracing configurations (Tahamouli-Roudsari et al. 2017).

2 Experimental program

2.1 Preliminary design of ESB retrofit for RC frame

The deformability of RC frame retrofitted with ESB largely depends on the geometric dimensions and reinforcement detailing of link beam; longer links provide high inelastic deformation capacity. Longer link also has the advantage of less affecting the initial stiffness of RC frame. If link detailing is sufficient to resist seismic shear force, RC link beam respond in a stable manner by developing flexure hinges at the link ends. The braces will be designed for the corresponding axial force to respond elastically. Assuming rigid behavior of frame and braces, the frame lateral drift θ can be formulated as proposed by Popov and Engelhardt (1988):

$$\theta = \frac{\gamma L_1}{L_{bay}} \tag{1}$$

where γ is the link rotation, L_1 is the length of link and L_{bay} is the bay length of frame. This equation assumes rigid behavior of both frame and braces. The axial deformation in brace will also contribute to the lateral drift of the frame (MacRae et al. 2004):

$$\theta_b = \varepsilon \frac{L_{bay}}{h} \tag{2}$$

where θ_b is the lateral drift of frame due to axial deformation in brace, h is the story height and ε is the elastic strain developed in brace. Since the tension and compression braces are intended to respond elastically for the developed inelastic actions of the system, the corresponding overstrength axial force will be always less than the yield force. Therefore, θ_b will be less than 0.15%, which may be ignored in the preliminary design. The yield drift of frame will be based on the yield moment developed in the link beam. For this purpose, the yield rotation of link beam can be related to the link yield curvature:

$$\gamma = \frac{\phi_y L_1}{6} \tag{3}$$

where ϕ_y is the yield curvature, as formulated by Priestley et al. (2007):

$$\phi_y = 1.70\left(\frac{\varepsilon_y}{h_b}\right) \tag{4}$$

where ε_y is the yield strain of longitudinal rebar of link beam and h_b is the depth of beam. The link rotation and the corresponding yield drift of frame can be approximated as:

$$\gamma = 0.30 L_1 \left(\frac{\varepsilon_y}{h_b}\right) \tag{5}$$

$$\theta = 0.30\left(\frac{\varepsilon_y}{h_b}\right)\left(\frac{L_1^2}{L_{bay}}\right) \tag{6}$$

The use of longer link will also facilitate accommodating openings for door and windows. The present research considered attaching brace to the beam at a distance of $L_{beam}/8$ i.e. the centerline of brace intersect the beam at a distance of 1/8th of beam length from the face of column. Further, assuming typical dimension of commonly used beam as 12 inch × 18 inch (205 mm × 457 mm) having Grade 60 rebars ($\varepsilon_y = 0.002$) and bay length of 18 feet (5.50 m), Eq. (6) gives yield drift of 0.40%. The retrofitted RC frame will be able to reach the maximum allowable drift of 2.50% before reaching the collapse limit state of link beam. However, such maximum capacity of frame drift will be required for maximum considered earthquake in case of ESB retrofitted RC frame. It is due to the fact that the use of braces in RC frame will reduce the inelastic deformation capacity of frame. For preliminary design of retrofit, the collapse prevention (CP) limit state drift is taken as 2.50% while the life safety (LS) limit state is taken as 2.0% ($\approx 0.75 \times 2.50$). Considering the LS limit state drift capacity of frame as the maximum drift for design base earthquake, the demand ductility μ will be equal to 4.94 ($\mu = 2.0/0.40$). Furthermore, assuming the initial time period of retrofitted braced frame to be less than 0.50 s, the response modification factor R of ESB retrofitted RC frame can be calculated as proposed by Newmark and Hall (1982): $R_\mu = (2\mu - 1)^{0.5} \approx 3.0$. The ASCE 7-16 (2016) also suggests overstrength factor Ω_o of 2.0 for eccentric frame buildings. However in case of retrofitting of existing frame this will not be known at the preliminary design stage. Moreover, the calculated ductility is based on approximate analytical model in comparison to a detailed model (Sullivan 2013) that takes into account other deformations due to shear deformation of link, shear and flexure deformation of beam outside the link, axial deformation of brace and columns in addition to rigid frame deflection and flexure deformations of link. In case of RC frame retrofitted with steel braces, additional deformation may arise from the improper contact between concrete surface and steel plates, and slippage of anchors, at connections attaching braces to the beam. These additional deformations will increase the yield drift of the frame; hence, decreases the ductility capacity of frame. This will be confirmed through quasi-static cyclic tests on ESB retrofitted frame panel. Therefore, ignoring the overstrength for the preliminary design of retrofit will be rational, and it will result in more conservative design. Thus, the preliminary design of braces for ESB retrofitted RC frame was carried out using the static force procedure with $R = 3.0$. Such design assumptions are

applicable to link beam possessing the required inelastic rotational capacity. In case of gravity-designed frames the bracing retrofitting techniques may need to be combined with other direct techniques e.g. CFRP (Mazza and Mazza 2019), for better performance. In present case, the link beam was proportioned and detailed according to the seismic provisions of ACI 318-14 (2014) for structural concrete, which is expected to develop plastic hinges with sufficient inelastic rotational capacity.

The present research considered a two-story one-bay archetype 2D RC frame, which was analyzed for the design of ESB retrofit (Fig. 1). The RC frames were assumed having beams with size of 12 inch×18 inch (205 mm×457 mm) and reinforced with 6#6 rebars (no. 6, 19 mm), and columns with size of 12 inch×12 inch (205 mm×205 mm) and reinforced with 8#6 (no. 8, 19 mm). Transverse ties having dia of 3/8 inch (9.5 mm) were provided at a distance of 3 inch center-to-center (76 mm) in beams and columns. Concrete with compressive strength of 4000 psi (27.60 MPa) and rebars with yield strength of 414 MPa and ultimate strength of 621 MPa were considered. These considerations were made which are common in the existing deficient building stock of RC frames. Seismic floor mass of 15 tonne was assumed for each floor. Considering the building on rock site "Type B" soil, located in highest seismic zone with PGA = 0.40 g for design base earthquake and taking $R = 3.0$, the seismic design spectrum of ASCE 7-16 gives maximum base shear coefficient of $0.33W$ where W is the seismic weight of the building.

For seismic upgrade of RC frame, hollow box section of A36 steel were considered with dimensions (depth, width, thickness) of 4.50 inch×4.50 inch×3/16 inch (114.30 mm×114.30 mm×4.76 mm). Table 1 shows the geometric and material properties of assumed hollow box section. The retrofitted RC frame was modeled in finite element based program SAP2000 (CSI 2014) for lateral load analysis under the design level base shear force of $0.33W$. The maximum axial and bending forces were calculated in the brace. The demand to capacity ratio of combined stresses in steel section was calculated as per the AISC 360-16 (2016):
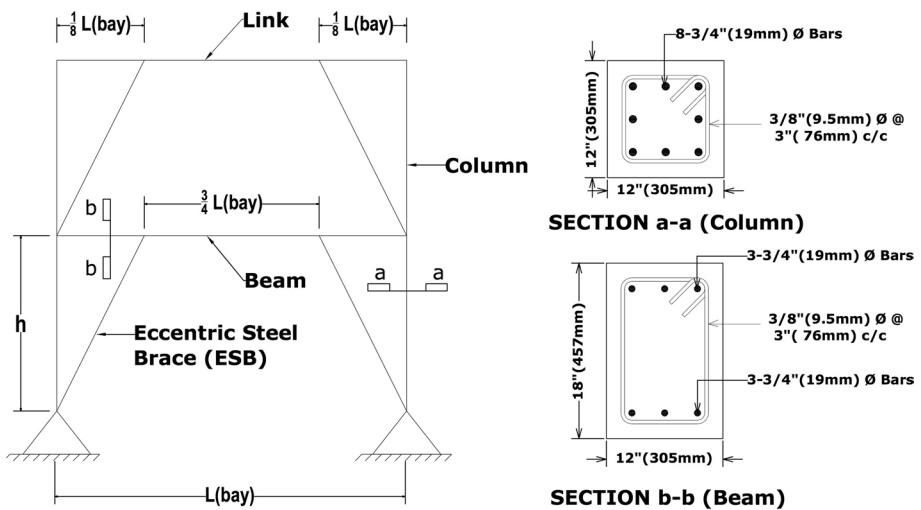

Fig. 1 Geometric and reinforcement details of two-story RC frame considered for retrofitting using eccentric steel braces (ESB). In the above figure, h = 12 ft (3050 mm) is the story height and L(bay) = 18 ft (4570 mm) is the bay length

Table 1 Geometric and material properties of HSS (114.30 mm × 114.30 mm × 4.76 mm) braces

Cross-sectional area, A	2025.80 mm^2	Moment of inertia, I$_{33}$	3,995,822 mm^4
Yield strength, f_y	248 MPa	Section modulus, S$_{33}$	69,918 mm^3
Ultimate strength, f_u	275 MPa	Radius of gyration, r$_{33}$	44.41 mm
Young modulus, E	200 GPa	Plastic modulus, Z$_{33}$	82426 mm^3

$$D/C = \frac{P_r}{P_c} + \frac{8}{9}\left(\frac{M_r}{M_c}\right) \tag{7}$$

where *D/C* is the demand to capacity ratio of combined axial and bending stresses in brace, P_r is the factored maximum axial force demand in brace, P_c is the axial capacity of brace, M_r is the factored maximum in-plane bending demand in brace and M_c is the in-plane bending capacity of brace. The analysis requires $P_r = 54$ kips (241 kN) and $M_r = 33$ kip-inch (3767 kN-mm). The axial and bending capacity of considered brace is 79 kips (352 kN) and 162.97 kip-inch (18,413 kN-mm), respectively. Equation (7) gives D/C ratio close to 1.0, thus, the proposed section is capable to respond in the elastic range for the considered lateral force. The proposed design is expected to ensure elastic response of braces till the CP limit state of link beam.

2.2 Quasi-static cyclic tests on portal frames

2.2.1 Description of test frames

For quasi-static cyclic testing, 1:3 reduced scale representative one-story one-bay portal frames were prepared. Only the ground-story panel was considered for testing and numerical calibration, however, the columns were extended up to the half of second-story. All the linear geometric dimensions of beam and columns and diameter of re-bars were reduced by a scale factor $S_L = 3.0$. Similarly, dimensions of braces were also reduced to 1.50 inch × 1.50 inch × 1/16 inch (38 mm × 38 mm × 1.60 mm). Figure 2 report details of the 1:3 reduced scale test frame model prepared for quasi-static cyclic testing. Brace-to-beam and brace-to-column base connections, and beam/column section details are also shown in Fig. 2. For brace-to-gusset plate connectivity, first a slot was created at each end of the brace in order to insert gusset plate into the brace, which was connected through 1/4 inch (7.94 mm) fillet longitudinal weld using electrode with strength of 60 ksi (414 MPa). The nominal strength and load capacity of longitudinal weld was calculated as per the AISC and LRFD design equations:

$$\text{Nominal strength of weld,} \quad F_w = 0.6F_{exx} \tag{8}$$

$$\text{Design strength of weld,} \quad \phi R_{n1} = 0.75\left(0.707aF_w\right) \tag{9}$$

$$\text{Shear rupture strength of base metal,} \quad \phi R_{n2} = 1.0\left(0.6tF_{ult}\right) \tag{10}$$

$$\text{Thickness of gusset plate for the corresponding weld,} \quad t_g = \frac{0.707aF_w}{0.40f_y} \tag{11}$$
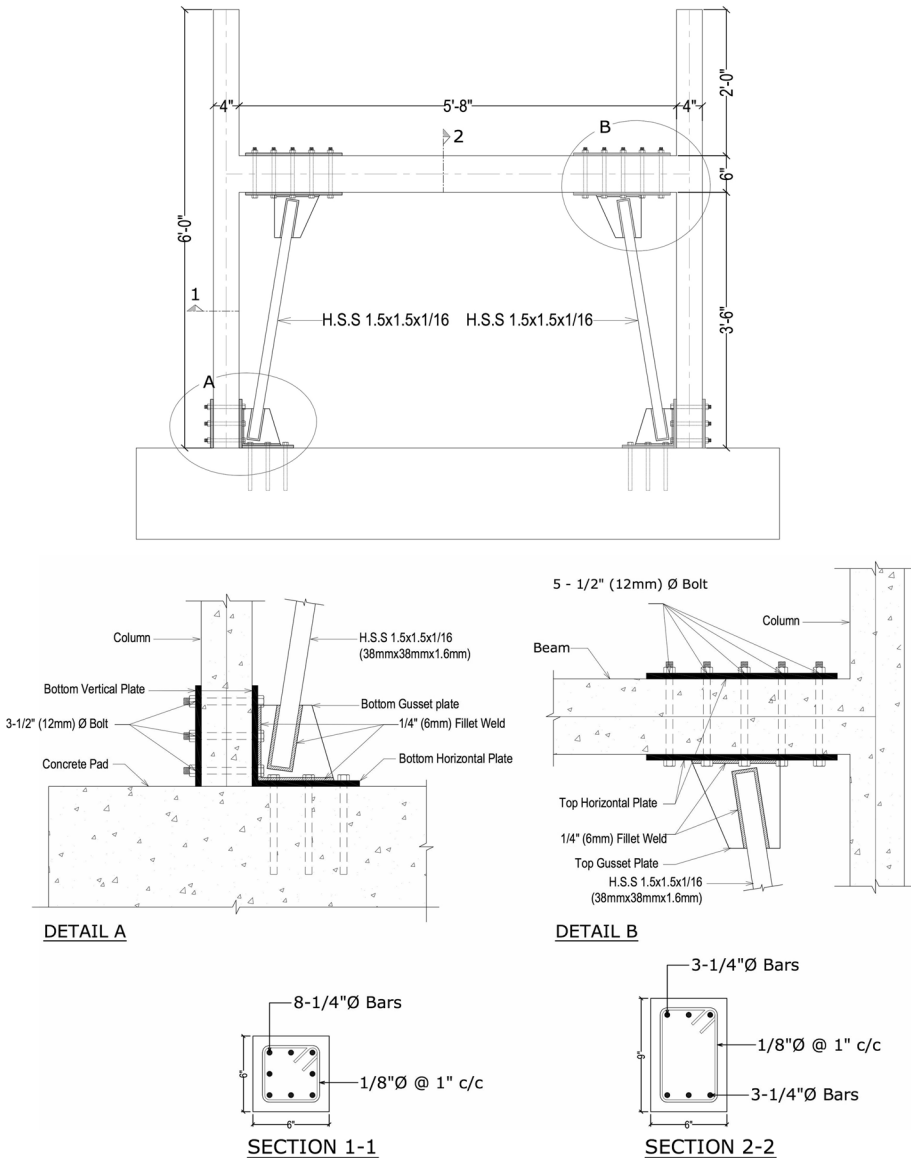
Fig. 2 Details of 1:3 reduced scale ESB retrofitted RC frame panel prepared for quasi-static cyclic tests

where F_W is the nominal strength of fillet weld, F_{exx} is the electrode strength, a is the fillet weld leg size that is 5/16 inch (7.94 mm), ϕR_{n1} is the design strength of weld, F_{ult} is the ultimate strength of base metal that was taken 54 ksi (373 MPa), t is the thickness of brae tube that is 3/16 inch (4.76 mm) for prototype and 1/16 inch (1.60 mm) for test model, ϕR_{n2} is the rupture strength of base metal, t_g is the thickness of the gusset plate, f_y is the yield strength of gusset plate material. Parallel longitudinal weld was applied over a total length of 16 inch (406.40 mm) in model that corresponds to 48 inch (1219.2 mm)

in the prototype. Considering the axial force demand under the design level forces in the brace, which was equal to 54 kips (241 kN), a factor of safety of 4.24 was achieved for the selected weld. Since, the thickness of the brace tube is generally lower, the safety factor against the shear fracture of base metal was also calculated that was found equal to 5.40. Such high factor of safety will ensure elastic behavior of weld and base metal even under extreme load in order to promote nonlinearity at other desired location of the structure. Similar weld length was used also for connecting gusset plate with the base plate that was attached to the beam. The gusset plate thickness was rounded to 18 mm for prototype and 6 mm for model, which was about 30% higher than the required thickness of gusset plate, calculated using Eq. 11. The thickness of base plate was approximated equal to the thickness of gusset plate. Such provision will ensure fracture of weld under extreme loads while keeping all other components of connection to behave elastically. Efforts were made to meet the requirements suggested by Roeder et al. (2011) for gusset plates, to approximate the size and shape of gusseted connections and required welding. The proposed retrofitting scheme requires the braces to be attached to the horizontal plates, which are placed below the beam, that is attached to another plate above the RC beam through anchors. The application of this retrofitting when a concrete slab is present will required additional cautions, which has not been discussed herein.

2.2.2 Test setup, instrumentation and loading protocols

A displacement-controlled hydraulic actuator was employed to subject the test frames to quasi-static cyclic lateral loads for multiple-levels of story displacements (Fig. 3). A 50-ton actuator was used, which comprised of a ram and a load cell. The actuator had a pin connection arrangement at both the ends, in order to eliminate any accidental eccentricity but allows small rotations. A rigid distribution beam was attached to the actuator, which itself was attached to test frame through clamps made of four steel rods connected to transverse beams. This arrangement was used in order to apply horizontal displacement without prestressing the beams.

The loading history for quasi-static cyclic tests was prepared as per the ACI ITG-5.1-07 recommendations (Fig. 4). The ACI ITG-5.1-07 requires the amplitude of first three cycles does not exceed 60% of the design displacement and also the maximum displacement of the subsequent cycles remains between 1.25 and 1.50 times the previous applied maximum displacement. The test models were subjected to three cycles at each level of story drifts.
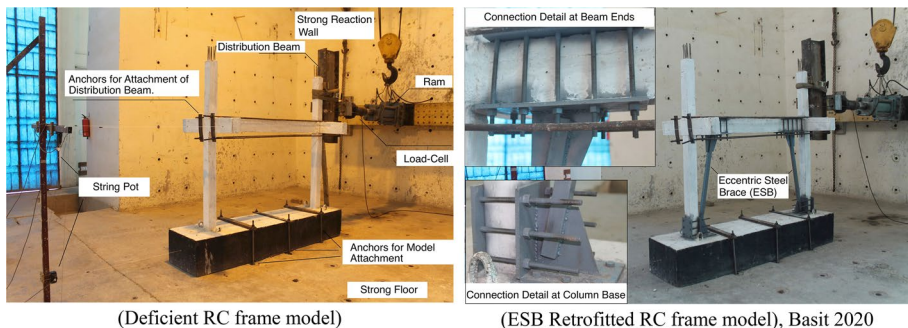

(Deficient RC frame model)　　　　　　　(ESB Retrofitted RC frame model), Basit 2020

Fig. 3 Quasi-static cyclic tests on as-built (left, Khan 2020) and ESB retrofitted (right, Basit 2020) frames
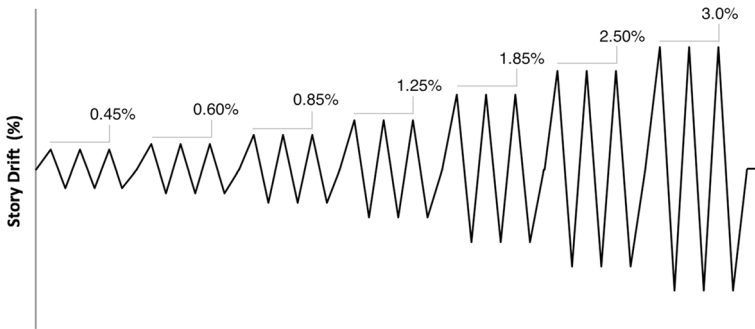
Fig. 4 Story displacement history for quasi-static cyclic loading of test models

The selected maximum roof drift corresponds to the code permissible story drift for low-rise structures. However, the drift level was further increased till the model was found in the incipient collapse state. Each model was tested progressively from elastic to ultimate state and was inspected for possible damages after each three cycles. The test models were instrumented with two displacement transducers (string pots) at beam story level to record lateral displacement response of frame. A displacement transducer was also installed at the base pad of model to record any possible horizontal sliding of test model.

3 Behaviour of deficient and ESB retrofitted RC frames

3.1 Observed damage mechanism of tested frames

Deficient RC frame During first test runs, flexure cracks were appeared in columns at the top end that distributed over a length of 22% of total length (0.22L, where L is total length of column members) during subsequent runs. Slight shear cracks appeared in joint under story drift of 0.75%. Slight flexure cracks also appeared at the beam ends under this run. Flexure cracks were observed at the base of columns under story drift of 1.10%. Additional cracks appeared in joint under this run. The existing cracks widened further under subsequent test runs. Cover spalling was observed at the base of columns under story drift of 2.75% and the shear cracks in joints widened further. The test model was found in the incipient collapse state at story drift of 3.73%. Under this test run, concrete cover spalling was observed at joints. Core concrete tension splitting was observed at the base of column due to shear failure. On inspection, it was found that lateral tie was displaced during concrete compaction process. The spacing of ties was doubled at this location. Figure 5 shows the observed damages of RC frame under increasing lateral drift demand.

ESB retrofitted RC frame In case of ESB retrofitted test model, initial flexure cracks appeared at the beam ends under first test run cycles. In subsequent runs, the flexure cracks in beam distributed over the beam at the location where braces were connected to beam. The model response was stable, exhibiting flexure hinging of beams till 1.94%. Flexure cracking was observed at the base of column, and slight in-plane bending was observed at the top end of one brace under story drift of 2.82%. Figure 6 shows the observed damages of ESB retrofitted RC frame under increasing lateral drift

Story Drift = 0.30%: Flexure yielding at the top end of column under connection opening.

Story Drift = 1.10%: Occurrence of shear cracks in joint under connection closing.

Story Drift = 1.10%: Flexure yielding of beam under connection closing.

Story Drift = 2.50%: Extensive flexure cracking at the top ends of columns.

Story Drift = 3.73%: Concrete cover spalling and core concrete tension splitting.

Story Drift = 3.73%: Concrete cover spalling at joint under connection closing.

Fig. 5 Observed major damages in deficient RC frames with increasing story drift demand

demand. The proposed scheme ensured the braces remain fully secured during entire loading. However, the attachment can be further improved through the application of epoxy-mortar.

Comparison of damage mechanism of deficient and ESB retrofitted RC frames The predominant damage mechanism of deficient RC frame was shear cracking of joints and flexure hinging of columns at both top and bottom ends, which was followed by cover spalling at the base of columns. As presumed in the preliminary design, the observed predominant damage mechanism of ESB retrofitted RC frame was flexure hinging with

Story Drift = 1.94%: Distribution of flexure yielding over the beam length at the location of brace connection.

Story Drift = 2.82%: In-plane bending of brace causing slight kink in brace.

Story Drift = 2.82%: A small kink was seen in brace due to in-plane bending at brace end.

Fig. 6 Observed major damages in ESB retrofitted RC frames with increasing story drift demand

stable cyclic response till the design level displacement (i.e. 2% story drift). The ESB retrofitted frame reached the incipient collapse state at a story drift of 2.82%.

3.2 Hysteretic force–displacement response and hysteretic damping

3.2.1 Hysteretic force–displacement response

The lateral displacement recorded through string pot at beam level and base pad were processed for baseline correction. The average of unbalance displacement was calculated, which was subtracted from each recorded displacement. The corresponding lateral force was calculated through load cell, which was also processed for baseline correction. The
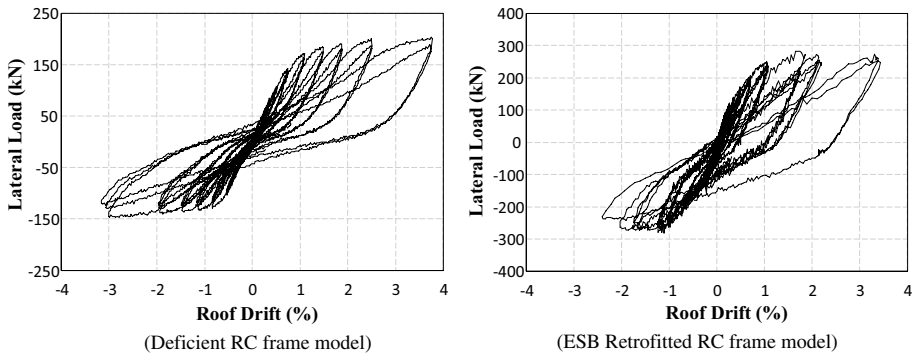
Fig. 7 Force-displacement hysteretic response of deficient and ESB retrofitted RC frame models
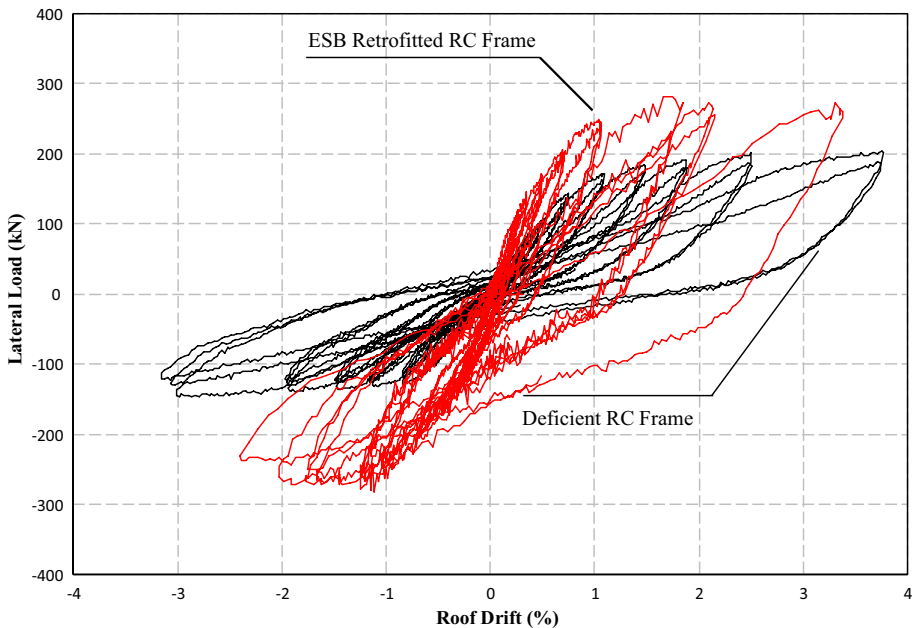

Fig. 8 Comparison of force–displacement hysteretic response of deficient and ESB retrofitted RC frame models

model force and displacement response was transformed to the prototype using the applicable conversion factors: scale factor $S_L = 3$ was used to transform displacement while scale factor $S_L^2 = 3^2$ was used to transform lateral force. The model base displacement was subtracted from the beam level displacement in order to calculate the model relative displacement. It was further normalized by the story height to calculate the corresponding story drift. Figures 7 and 8 shows the hysteretic response of both deficient and ESB retrofitted RC frames. The ESB retrofitted frame has exhibited high initial stiffness and high peak resistance compared to deficient RC frame. The deficient frame has exhibited maximum

lateral resistance of 204 kN while this increased to 282 kN in case of ESB retrofitted frame, which indicates an increase of about 38% in the lateral strength of frame. An increase of 91% was observed in the initial stiffness of the frame. The hysteretic response of deficient RC frame was observed with pinching in the middle compared to the ESB retrofitted RC frame. The pinching behavior was due to the flexure hinging of columns and shear cracking of joints. This behavior was manifested also in the hysteretic damping of frames, discussed later in the paper.

3.2.2 Hysteretic damping

The concept of dissipated energy in a cycle to input energy has been used for calculating the hysteretic damping ξ_{hyst} of frames:

$$\xi_{hyst} = \frac{E_{diss}}{2\pi E_{in}} \tag{12}$$

where ξ_{hyst} is the hysteretic damping of system under a given cycle, E_{diss} is the energy dissipated by the system undergoing complete cyclic displacement (one-cycle) and E_{in} is the input energy to the system. The total area under the hysteretic cycle was calculated using the trapezoidal rule to measure E_{diss}, which is averaged over the three cycles. E_{in} was calculated for each cycle by calculating area under the curve for the equivalent elastic response of the system. The calculated hysteretic damping was correlated with the roof drift to study the variation of energy dissipation with damage progression in structure (Fig. 9). Initially both the deficient and retrofitted frames exhibited decrease in damping with increasing drift, which was due to unsymmetrical response of model in push/pull. Since, the occurrence of damage was relatively more in one direction compared to the other. The damping
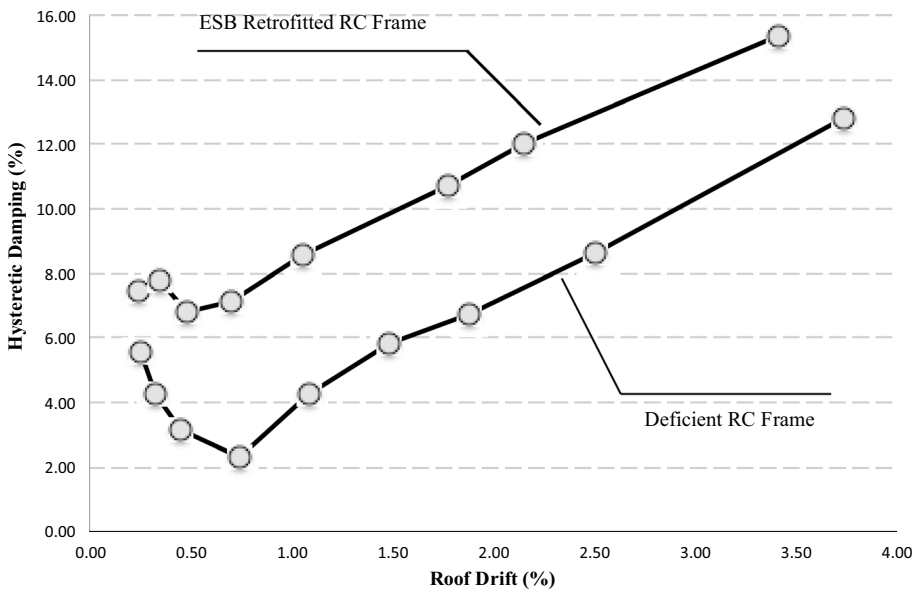

Fig. 9 Hysteretic damping of both deficient and ESB retrofitted frames

exhibited a linear increasing trend with increasing story drift demand when both the sides of frame incurred approximately the same damage. On average, hysteretic damping of 6% was observed for deficient RC frame, which increased to 10% in case of ESB retrofitted frame. This indicates the beneficial role of beam hinging in ESB retrofitted frame compared to the column hinging and joint cracking observed in the deficient RC frame.

3.3 Performance levels for deficient and ESB retrofitted frames

3.3.1 Lateral force—deformation capacity curves

The peak roof displacement and the corresponding peak force for both push and pull loading was identified, which were averaged over the three cycles for each test. The average lateral load was correlated with the relative story drift to derive average capacity curves. Figure 10a shows the mean capacity curves for both deficient and ESB retrofitted frames. The ESB retrofitted frame has exhibited high initial stiffness and high lateral resistance compared to deficient RC frame. The retrofitting decreased the ultimate displacement capacity but this doesn't necessarily cause reduction in the frame ductility.
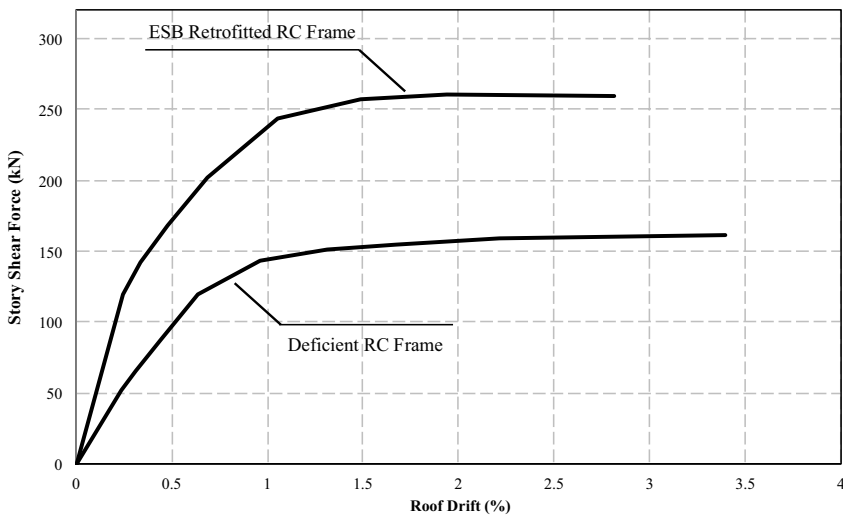
(a) Lateral force-displacement capacity curves of both deficient and ESB retrofitted frames
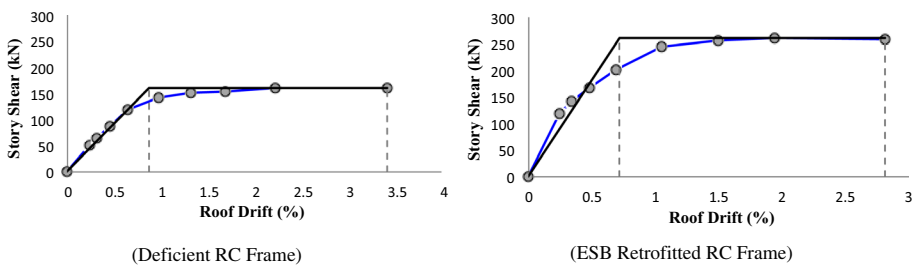
(b) Elastic-plastic idealization of capacity curves for both deficient and retrofitted RC frame

Fig. 10 Lateral force–displacement capacity curves and elastic–plastic idealization

3.3.2 Story drift limit states of test frames and damage scale

Drift limits were established for both the deficient and ESB retrofitted frames as per the performance levels given in FEMA-356 (2000) i.e. Immediate Occupancy (IO), Life Safety (LS) and Collapse Prevention (CP) limit states. The observed ultimate displacement capacity of frames was considered as the CP limit state drift capacity, because both the frame were found in the incipient collapse state for this drift demand. The LS limit state drift was taken as 75% of the CP drift level. The IO level in present study approximately corresponds to the initiation of flexure yielding in columns and beams in case of deficient and ESB retrofitted RC frame, respectively. Table 2 reports damage scales developed for both the deficient and ESB retrofitted frames. Considering the LS limit state as the design base limit state, Table 2 shows that the design base story drift of ESB retrofitted RC frame can be taken as 2.0% ($2.12\% \approx 2.0\%$), which is in agreement with the preliminary design consideration.

3.3.3 Elastic–plastic idealization of capacity curves

The lateral force–deformation capacity curves of the frames were bi-linearized using the energy balance criterion. The maximum displacement capacity observed in test was considered as the ultimate displacement capacity of the models. The idealized yield strength and yield displacement were calculated through iterative procedure that equalized the area under the idealized elastic–plastic capacity curve to that of area under the actual force–deformation curve. Figure 10b shows the idealized elastic–plastic curves for both the deficient and ESB retrofitted RC frames. The ESB retrofitting primarily increased the yield stiffness and yield strength of frame by 100% and 60%, respectively. The deficient frame exhibited maximum ductility of 3.91, which increased to 3.97, exhibiting only a marginal increase due to ESB retrofitting. It is worth to mention that this maximum ductility corresponds to the CP limit state. Ductility capacity of tested frames can be approximated as 3.0 and 3.50 for deficient and ESB retrofitted frames respectively, considering LS limit state as the design base limit state. The observed yield drift capacity of ESB retrofitted frame is 0.70%, which is 75-percent higher than the value calculated using simplified analytical drift model (Eq. 6). It is due to the fact that the simple model has ignored contribution of shear deformation of link beam, flexure and shear deformation of beam outside link, axial deformation of braces and columns, and contribution of longitudinal re-bars slip/pullout in beam that is common in RC frames having concrete with low strength (Ahmad et al. 2018). This suggests increasing the multiplying factor from 0.30 to 0.50 in Eq. (6). The modified drift model also takes into account possible deformation due to improper contact between concrete surface and steel plates, and slippage of anchors, at connections attaching braces to beam. As expected, the resulting ductility of frame reduced from 4.94 to 3.5 exhibiting 41% reduction.

3.4 Analytical lateral strength of ESB retrofitted RC frame

The global equilibrium of frame requires the external lateral force causing overturning moment (OTM) demand on frame must be equilibrated by internal forces:

$$(OTM)_{external} = Fh \tag{13}$$

$$(OTM)_{internal} = 2M_c + VL_{bay} \tag{14}$$

Table 2 Performance levels and damage states of deficient and ESB retrofitted RC frames. The drift limits were established based on observed experimental response

Models	Parameters	Performance levels		
		Immediate occupancy	Life safety	Collapse prevention
Deficient RC frame	Drift (%)	0.61	2.55	3.40
	Damages	Initiation of flexure yielding in columns	Existing flexure cracks in columns widens further. Flexure cracks distributed over length of (0.22L) in column. Significant cracks occur in joints	Existing cracks in joints further aggravates. Concrete cover starts spalling at joint. Cover spalling and core crushing observed at the base of columns. The frame is in the incipient collapse state
ESB retrofitted RC frame	Drift (%)	0.50	2.12	2.82
	Damages	Initiation of flexure yielding in beams at the location of eccentric braces.	Existing flexure cracks in beams further widens. Flexure cracks in beams were distributed over the location where brace was attached i.e. 0.13L	Existing cracks in beams further aggravated. Minor cover spalling observed at the beam-ends. Slight bending was observed at the end of brace

$$V = \frac{2M_B}{L'} \tag{15}$$

where F is the lateral force required to develop plastic hinges at all the desired locations, h is the story height, $M_{C,i}$ is the plastic hinge capacity of column at base, V is the shear force developed in beam corresponding to the maximum moment capacity M_B of plastic hinges in beam, L' is the length of link beam. Equation (14) considers that plastic hinges will form in beam, and also, plastic hinges will be permitted to form at the column base to complete the designed required beam-sway mechanism of frame. In present case, $M_B = 190$ kN-m and $M_C = 140$ kN-m were calculated through moment–curvature analysis of each section in SeismoStruct, taking into account material overstrength of 1.70 for compressive strength of concrete and 1.30 for yield strength of re-bars. Such consideration corresponds to the maximum feasible strength in plastic hinges for capacity design calculations (Priestley et al. 2007). $L' = \frac{3}{4}L_{bay}$, where L_{bay} is the bay length.

The above global equilibrium consideration gives estimate of lateral strength of 230 kN for ESB retrofitted RC frames, which is about 11% less than the maximum strength of tested frame. However, such discrepancy is justifiable realizing the simplified nature of analytical procedure. Equations (13) to (15) can be used in combination with Eq. (6), with the appropriate adjustment as discussed earlier, to construct lateral force–displacement capacity curve for single-story portal frame (Fig. 11). These are extendable also to similar frame with multi-stories, which can facilitate design and assessment of ESB retrofit for deficient RC frames.

4 Seismic performance evaluation of ESB retrofitted RC frame

4.1 Calibration of FE based numerical models

The prototype of test frame was prepared in the finite element based software Seismo-Struct, which included fiber-section based nonlinear models for static and dynamic seismic analysis of frame structures (Pinho 2007). The beam-column members and braces were modeled with beam-column element available in SeismoStruct that uses the inelastic force-based formulation (Spacone et al. 1996; Neuenhofer and Filippou 1997). Members with 4-element subdivisions were used, considering 15% of total member length for both
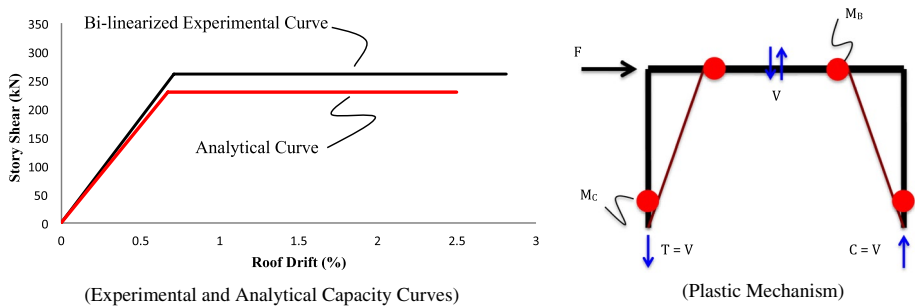

(Experimental and Analytical Capacity Curves)   (Plastic Mechanism)

Fig. 11 Comparison of analytical to experimental capacity curve (bi-linearised) for ESB retrofitted RC frame

ends subdivisions. Each integration section of element was considered with 200 section fibers. This element is capable of modeling both the material inelasticity, simulating the spread of plasticity over the length of member, and geometric nonlinearity of members under cyclic actions (displacement, rotation) for simulating the bending and axial response of element. The element can account for the effect of axial load on the moment capacity. The reinforced sections of beam-column members were modeled using the Mander et al. (1988) constitutive relationships for modeling behavior of confined/unconfined concrete, and using the Giuffre-Menegotto-Pinto (Filippou et al. 1983) constitutive relationships for modeling behavior of rebars. Material overstrength factors of 1.70 and 1.30 were considered for concrete and rebars, respectively. The braces were modeled using the inbuilt hollow structural section (HSS) $HSS_{4\text{-}1/2 \times 4\text{-}1/2 \times 3/16}$ available in SeismoStruct, which was assigned with bi-linear constitutive relationship for S235 steel material considering yield strength of 36 ksi (250 MPa). The current modeling ignored local/global buckling behavior of braces. It is due to the facts that the initial design assumed elastic behavior of braces till the plastic hinges develop their maximum capacity, and also, except the slight in-plane bending no any global/local buckling of braces were noticed till the ultimate drift demand. Furthermore, joint shear hinging was not considered in case of the ESB retrofitted frame, since the provision of braces ensured plastic hinges in beam and didn't cause any substantial damage in joints or columns.

The numerical model was subjected to lateral displacement history at the beam level, which was compatible with the peak displacement (push/pull) measured experimentally, and using the static time history analysis procedure given in SeismoStruct. Figure 12 reports comparison of the numerically predicted to experimentally observed lateral force–displacement hysteretic response of ESB retrofitted frame. For the clarity purpose, only the post-yield cycles were considered for comparison. The comparison have revealed that the proposed modelling technique can reasonably simulate force–displacement hysteretic response of frame in terms of maximum resistance, loading/unloading stiffness and in-cycle strength degradation. Most suitable parameters found through calibration for Giuffre-Manegetto-Pinto are: $R_0 = 19$, $b = 0.005$, $A_1 = 18.50$, $A_2 = 0.15$, $A_3 = 0.025$, $A_4 = 1$.

Furthermore, axial forces and in-plane bending were obtained for both left and right brace, which was normalized by the nominal capacity to calculate the demand to capacity (D/C) ratio (Figs. 13, 14). A maximum of $(D/C)_{axial} = 0.75$ was obtained for axial force in brace while maximum $(D/C)_{bending} = 0.96$ was obtained for bending in braces. D/C ratio
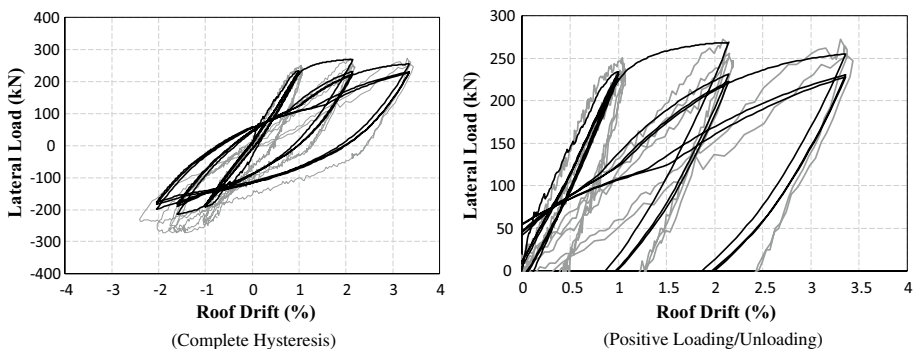

Fig. 12 Numerical (dark colour) to experimental (grey colour) comparison of lateral force–displacement hysteretic response of ESB retrofitted frame. Only post yield cycles are shown for clarity
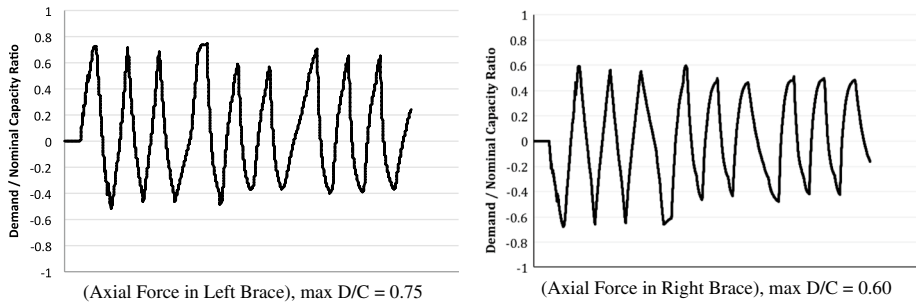
(Axial Force in Left Brace), max D/C = 0.75

(Axial Force in Right Brace), max D/C = 0.60

Fig. 13 Ratio of axial force demand to nominal axial capacity of brace. The ratio less than 1.0 indicates elastic response of brace

(Bending in Left Brace), max D/C = 0.86
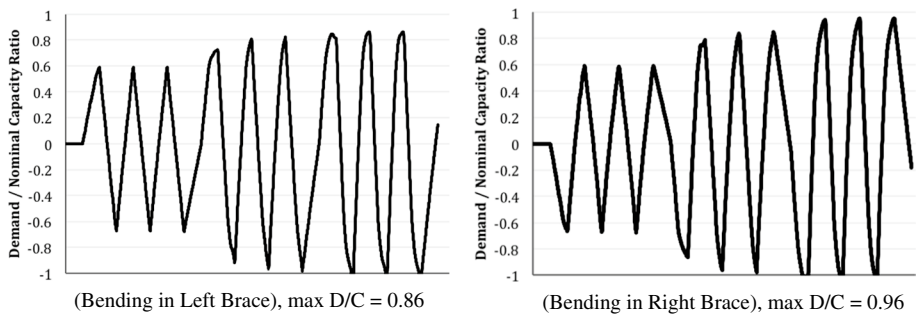
(Bending in Right Brace), max D/C = 0.96

Fig. 14 Ratio of bending demand to nominal bending capacity of brace. The ratio less than 1.0 indicates elastic response of brace

less than 1.0 indicates elastic response of brace. In present case, the braces have factor of safety of 1.33 for axial yielding and 1.04 for flexure yielding. The proposed design has ensured elastic response of brace against both the axial and bending demand, however, the bending capacity of braces is higher than the demand only by a margin. Since, $(D/C)_{bending} > (D/C)_{axial}$ this indicates that the braces will first yield in flexure. The same has been confirmed also by the experimental response of test model (Fig. 6). In addition to this, using Eq. (7) for calculating D/C ratio in brace as per the AISC 360-16 (2016), D/C becomes equal to 1.42 for ESB retrofitted frame under ultimate drift demand. This indicates the expected inelasticity in brace due to combined stresses under ultimate drift demand. However, such high level of drift demand on ESB retrofitted frame is very unlikely to exceed even in a maximum considered earthquake.

4.2 Response modification factors of ESB retrofitted two-story RC frame

The nonlinear modeling technique was extended to ESB retrofitted two-story RC frame. The model was assigned with nodal seismic mass of 14 ton at each floor. Initially, the frame was analyzed through eigenvalue analysis for the computation of natural period and the associated nodal displacements. The fundamental time period of 0.40 s was obtained for first mode. The corresponding nodal relative displacement obtained were 1.0 and 0.50 at the roof and first-floor level, respectively. This indicates linear deflected shape of structure,

which was expected for ESB retrofitted RC frame. The first-mode nodal displacements obtained were applied as a lateral displacement vector on the structure. The structure was displaced laterally through static displacement controlled pushover analysis up to a target roof drift of 2.0%. The first plastic hinge in beam was formed at a lateral load of 142 kN, however, the peak lateral resistance of structure reached to 265 kN (Fig. 15), exhibiting significant behavior. This is due to the fact that plastic hinges do not form simultaneously in all beams in eccentric braced frames (Tapia-Hernandez and Garcia-Carrera 2019). This indicates an overstrength $\Omega_0 = F_{max}/F_{plastic-hinge} = 265/142 \approx 1.86$, where $F_{plastic-hinge}$ is the lateral force corresponding to the first plastic occurrence in beam. The calculated overstrength factor $\Omega_0 = 1.86$ is in good agreement with the suggested overstrength factor of ASCE 7-16 (2016) for eccentric braced frame. The capacity curve of structure was bi-linearized in accordance with the FEMA P695 procedure. The structure ductility μ was found equal to 2.37, considering the maximum roof displacement corresponding to the peak force of structure. Furthermore, the fundamental time period of structure for first mode $T_1 = 0.46$ s. However, the time period corresponding to effective stiffness is greater than 0.50 s. This suggests ductility factor of $R_\mu = \mu = 2.37$. This gives total response modification factor $R = \Omega_0 \times R_\mu = 1.86 \times 2.37 \approx 4.41$ for ESB retrofitted two-story RC frame. The calculated R factor for ESB retrofitted frame is 47% higher than the initially taken $R = 3.0$ in the preliminary design of steel braces. This increase is due to the additional overstrength provided by the hardening behavior exhibited by the braced frame system.

4.3 Verification of ESB retrofit design for two-story RC frame

4.3.1 Selection of acceleration time histories

Acceleration time histories were extracted from the PEER strong ground motions database NGA-West2, which included acceleration time histories for active tectonic regimes with shallow crustal earthquakes. Acceleration spectrum was developed in accordance with the ASCE 7-16 to generate target design spectrum. The spectral response acceleration at short period $S_{DS} = 1.0$ and spectral acceleration at long period $S_{D1} = 0.4$ were taken to develop acceleration spectrum with design PGA = 0.40 g for design level earthquakes having 10% probability of exceedance in 50 years with 475 years of return period. The following search parameters were taken to search for list of appropriate acceleration time histories:
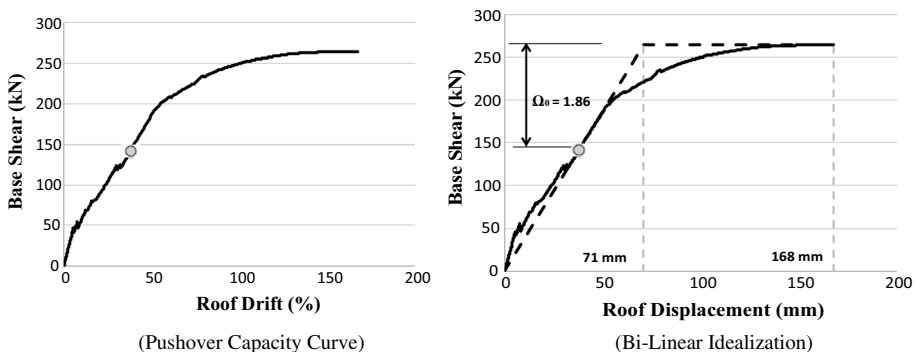

Fig. 15 Capacity curve developed for two-story frame through pushover analysis of frame in SeismoStruct

$M_W = 6.50$ to 7.50, $R_{jb} = 10$ to 30 km, fault mechanism = reverse/oblique, Vs30 = 360 to 760 m/sec, Duration = 15 to 60 s. A suite of 07 acceleration time histories was extracted (Table 3), which were further processed for scaling and matching. First, the scale factors suggested by the online tool of PEER for the selected time histories were used to linearly scale the acceleration records. Second, the linearly scaled accelerograms were matched to the design spectrum through wavelet-based procedure given in SeismoMatch. Spectral matching was carry out between T = 0.02 s to 2.0 s. A tolerance of 0.30 was taken to minimize the average misfit that was found to be 7.53%, considering average of misfit for all time histories. Figure 16 shows the comparison of design spectrum with the average acceleration spectrum developed for the selected matched acceleration time histories.

4.3.2 Nonlinear time history analysis (NLTHA)

The FE based numerical model for two-story frame was assigned with 2% elastic damping at the fundamental time period of frame, which was defined as a tangent stiffness proportional damping using Rayleigh model. This level of elastic damping has shown reasonable performance in predicting the time history response of RC frame (Ahmad et al. 2018). For nonlinear analysis, the Hilber-Hughes-Taylor (HHT) integration scheme was used with integration parameters of $\beta = 0.3025$, $\gamma = 0.60$ and $\alpha = -0.1$. The combined displacement/rotation and force/moment based criterion with limits 0.10 mm/0.0001 rad and 0.001 kN/1 kN-mm respectively were used, considering maximum tolerance of 1e20, to check for numerical instability of solutions. The analysis considered both the material inelasticity and geometric nonlinearity.

The ESB retrofitted RC frame was subjected to the matched acceleration time histories for seismic performance assessment of retrofitted frames under design base earthquakes (DBE). The matched acceleration time histories were further scaled linearly by a factor of 3/2 to approximate the acceleration time histories for maximum considered earthquakes (MCE), as suggested in ASCE 7-16 for relating MCE based response acceleration with DBE based response acceleration for seismic design. Figures 17 and 18 report the time histories of roof displacement response under DBE and MCE based acceleration time histories. Peak inter-story drifts were obtained for both DBE and MCE based acceleration histories (Figs. 19, 20). NLTHA for both the DBE and MCE based acceleration histories have

Table 3 Acceleration time histories extracted from the PEER NGA-West2 strong ground motions database

| Record	Earthquake name	Year	Station name	M_W	R_{jb} (km)	Component	PGA (g), scaled
1	San Fernando	1971	Santa Felita Dam (Outlet)	6.61	24.69	FSD262	0.45
2	Loma Prieta	1989	Coyote Lake Dam—Southwest Abutment	6.93	19.97	CYC285	0.56
3	Northridge-01	1994	Sunland—Mt Gleason Ave	6.69	12.38	GLE170	0.32
4	Cape Mendocino	1992	Loleta Fire Station	7.01	23.46	LFS270	0.44
5	San Simeon_ CA	2003	San Antonio Dam—Toe	6.52	16.17	36258021	0.44
6	Chuetsu-oki_ Japan	2007	Joetsu Ogataku	6.80	16.77	65011NS	0.32
7	Iwate_ Japan	2008	Semine Kurihara City	6.90	28.90	54026EW	0.36
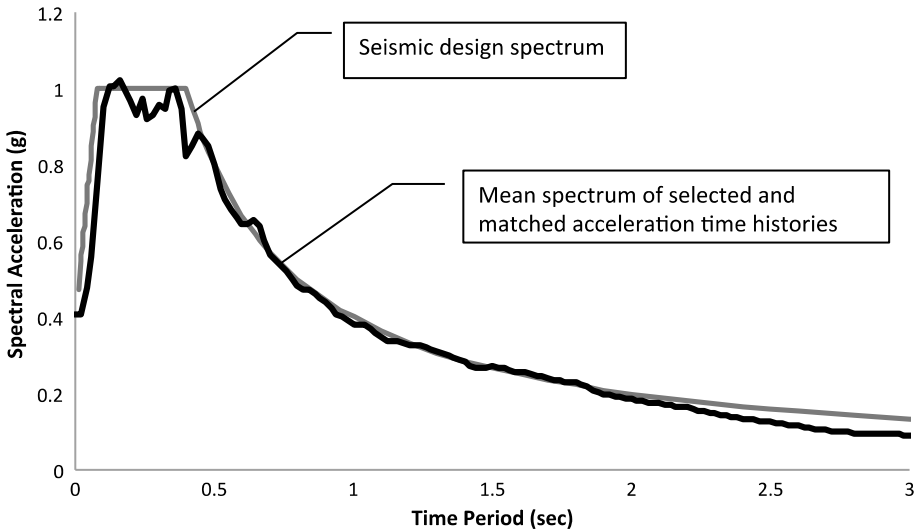
Fig. 16 Comparison of mean spectrum of matched acceleration time histories with seismic design spectrum given in ASCE 7-16 for site with design PGA = 0.40 g, S_{DS} = 1.0 g and S_{D1} = 0.40 g
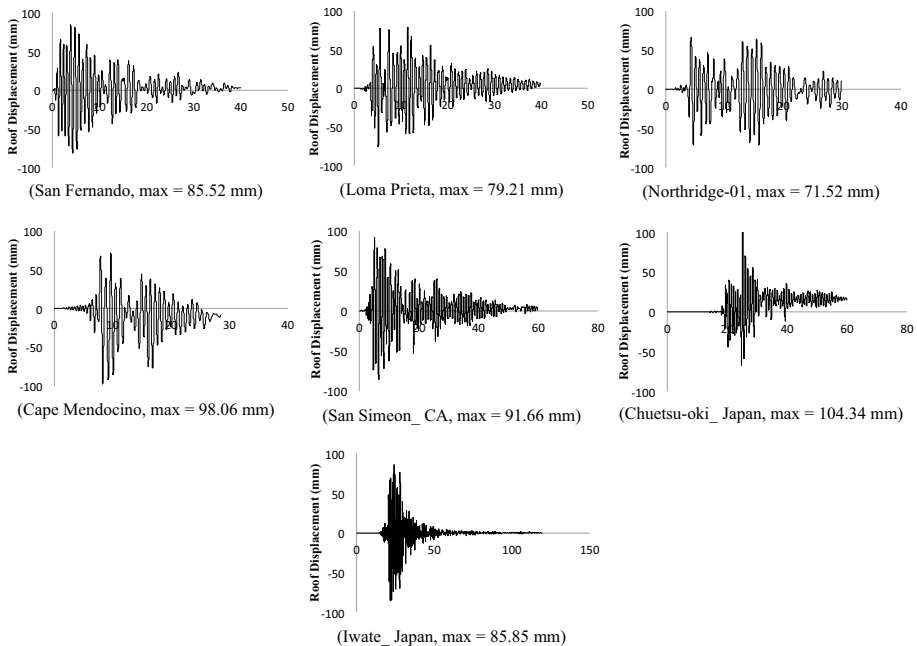

Fig. 17 Relative roof displacement response history under design base earthquakes

revealed linear pattern of inelastic deflected shape of ESB retrofitted RC frames. This supports the idea of imposing linear pattern of lateral displacement in the pushover analysis. On average maximum inter-story drift demand of 1.30% and 1.80% were obtained for DBE
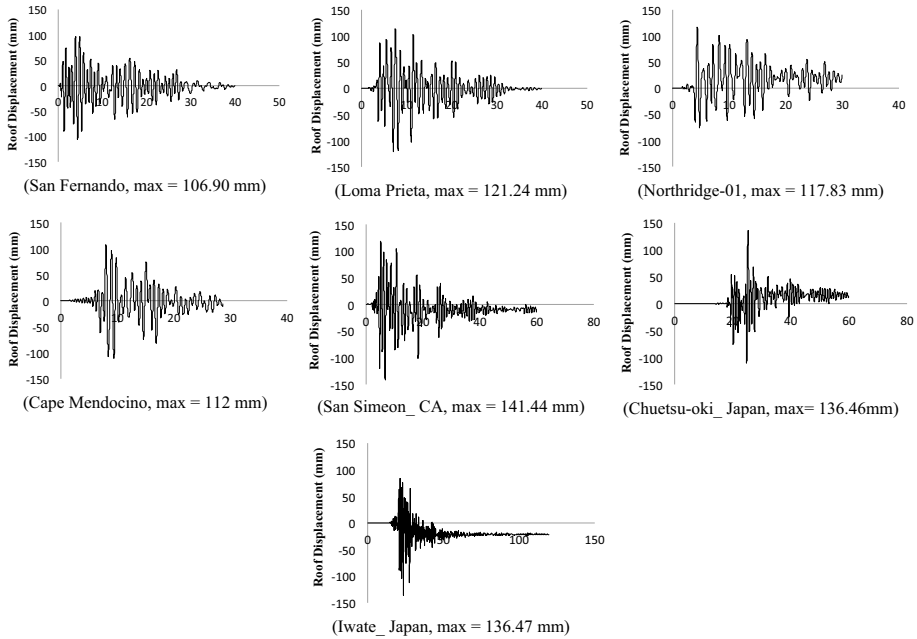
Fig. 18 Relative roof displacement response history under design maximum considered earthquakes

and MCE, respectively (Fig. 21). This gives drift demand to capacity ratio of 0.61 and 0.64 respectively, exhibiting significant safety margin. This indicates that the ESB retrofit for the considered RC frame can be further economized. However, considering the facts that possible uncertainties may be expected in actual seismic demand in the field and seismic response of structures, therefore, such higher safety margin will be favorable to ensure the structure perform satisfactorily in the field.

5 ESB retrofit of multi-stories RC frames

5.1 Design of ESB retrofit for multi-stories RC frames

In response to the growing interest in selective retrofit of RC frames (FEMA-547, 2006), direct internal steel braces offer an efficient alternative to enhance global stiffness and strength of structure. This can also reduce the cost of new designed structure by reducing seismic action demands on other components i.e. columns and joints. The present study considered RC frames having 3, 4, 5 and 6 stories (Fig. 22), which were analyzed and design in accordance with the ASCE 7-16 (2016) and AISC 360-16 (2016). The RC frames were considered to be located in highest seismic zones on rock site "Type B" with design level ground motions having PGA = 0.40 g, S_{DS} = 1.0 g and S_{D1} = 0.40 g. Assuming a linear displacement profile, the global ductility capacity fairly remains equal to story level ductility. Furthermore, nonlinear time history analysis performed herein on ESB retrofitted two-story frame designed with R = 3.0 have achieved significantly less D/C ratios of 0.61 and 0.64 for drift demand under design base and maximum considered earthquakes,
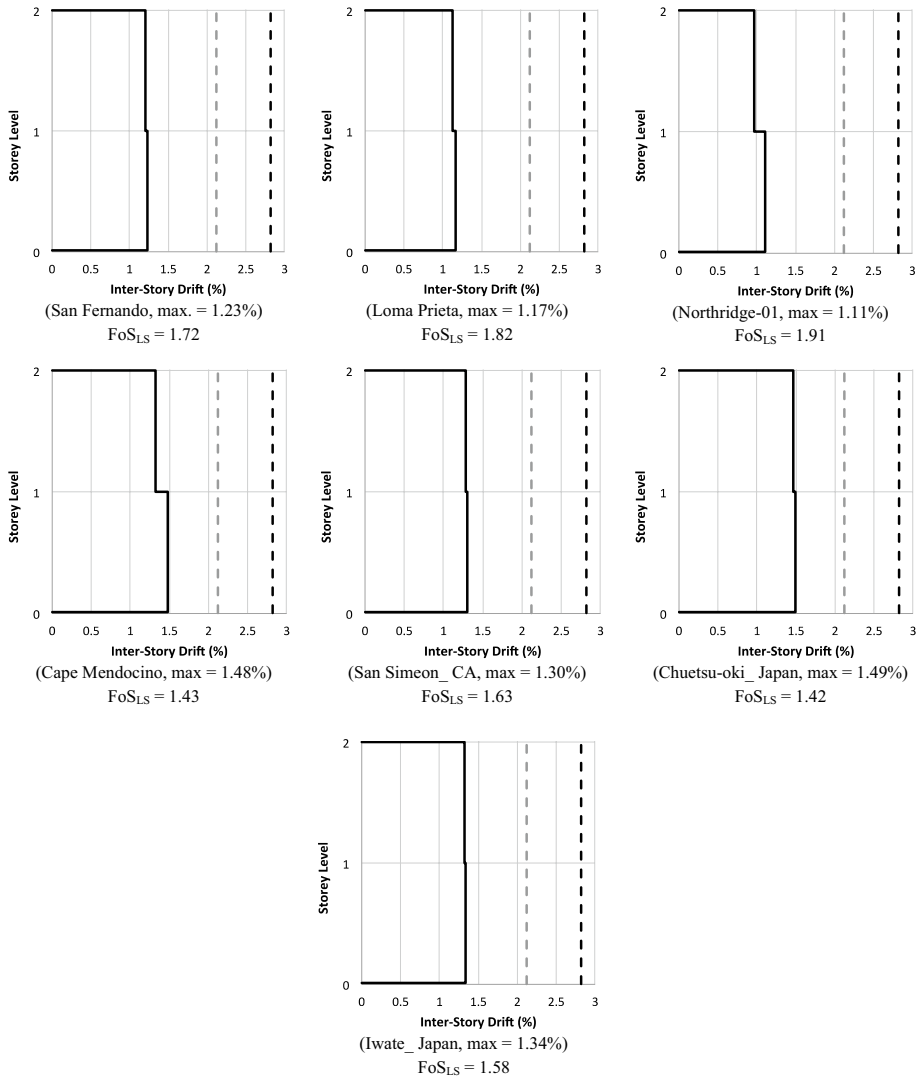
Fig. 19 Inter-story drift demand under design base earthquakes. The story-drift capacity corresponding to LS (grey line) and CP (dark line) drift limits are also shown. Factor of safety (FoS) against the LS level is also reported

respectively. Therefore, the consideration of $R = 3.5$ is deemed to be reasonable for seismic analysis and design of multi-stories ESB retrofitted RC frames. Lateral load analysis of frames was carried out in finite element program SAP2000 for calculating seismic actions in structural components. The geometric, material and dynamic properties of considered RC frames are reported in Tables 4 and 5. The design of steel braces involved the calculation of demand-to-capacity ratio of combined stresses due to axial and bending demand as per the AISC 360-16, which was ensured to remain equal or less than 1.0. It was found through the design that the same hollow box section of A36 steel with dimensions (depth, width, thickness) of 4.50 inch × 4.50 inch × 3/16 inch (114.30 mm × 114.30 mm × 4.76 mm)
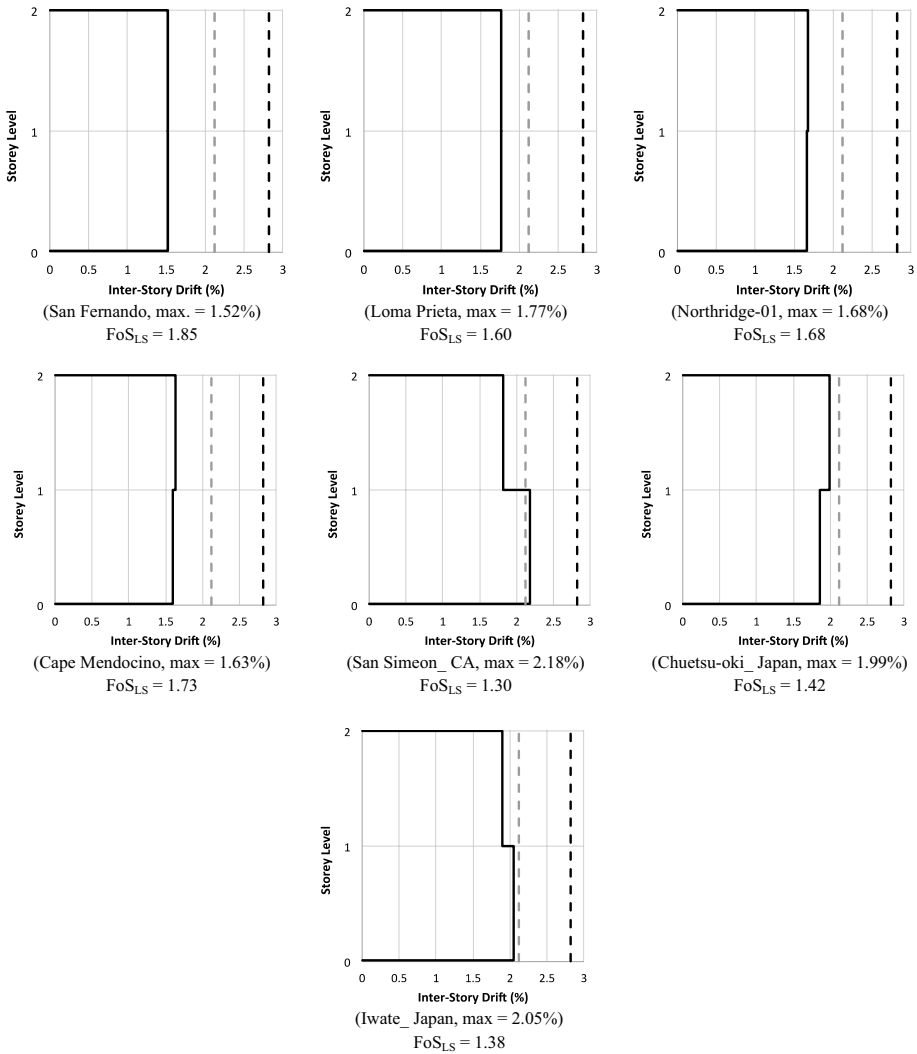
Fig. 20 Inter-story drift demand under maximum considered earthquakes. The story-drift capacity corresponding to LS (grey line) and CP (dark line) drift limits are also shown. Factor of safety (FoS) against the CP level is also reported

(Table 1) is sufficient for RC frame having 3 to 5 stories. It was found slightly higher than 1.0 on ground floor for 6 story frames, however, the same section was used for all floors. The beams and columns were designed for flexural demands to resist at least 25% of the seismic actions. This will require beams with less strength that will produce a more favorable ductile flexure mechanism of beams in the ESB retrofitted RC frame. However, the shear design of beams and columns should be carried out for lateral force level that develops the design level forces in braces. It is worth mentioning, the maximum lateral force capacity and subsequently developed shear forces in beams and columns members are controlled by the overstrength flexural capacity of the link members. However, the dynamic magnification effects may also alter developed actions in response history analyses.
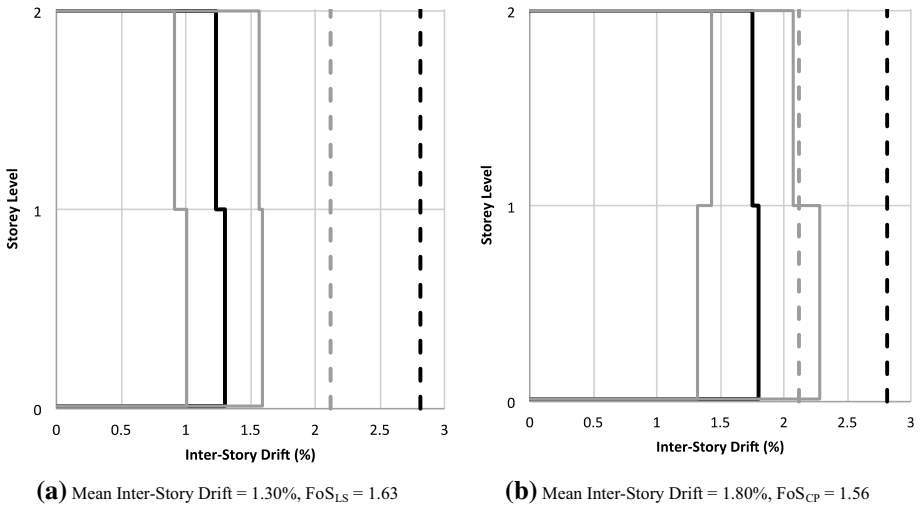
(a) Mean Inter-Story Drift = 1.30%, FoS$_{LS}$ = 1.63   **(b)** Mean Inter-Story Drift = 1.80%, FoS$_{CP}$ = 1.56

Fig. 21 Average inter-story drift demand under design base earthquakes (left) and maximum considered earthquakes (right). The story-drift capacity corresponding to LS (grey line) and CP (dark line) drift limits are also shown. Factor of safety (FoS) against the LS and CP levels are also reported. Average inter-story drift demands corresponding to 5th and 95th percentile are also shown
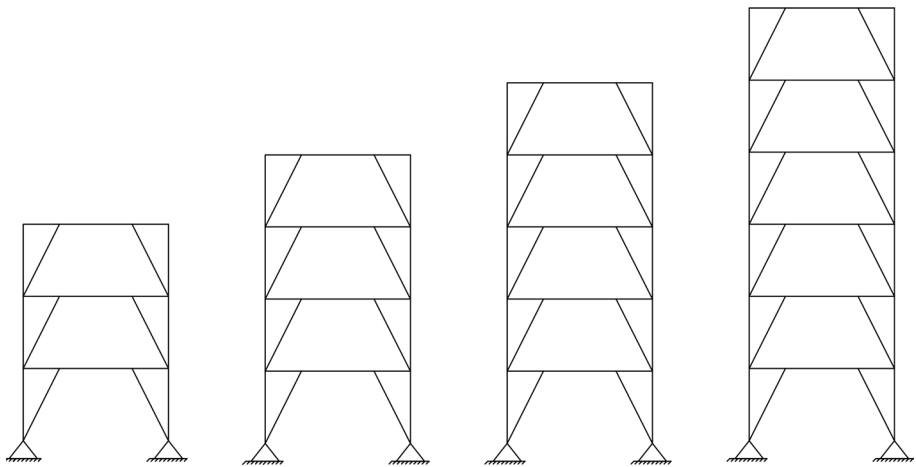

Fig. 22 Selected ESB retrofitted RC frames for design and verification

5.2 Response modification factors of ESB retrofitted multi-stories RC frames

The modeling technique was extended for preparing finite element base nonlinear numerical models for 3, 4, 5 and 6 stories ESB retrofitted frames. Results from the two-story frame are also presented. Initially, Eigen value analysis was performed on each model for calculation of modal frequencies and nodal displacements. Fundamental time period of each model is presented in Col. 2 of Table 6. These were compared also with the time period calculated using the empirical period model given in the ASCE-7-16 (2016)

Table 4 Geometric and material properties of RC frames

Property	Value
Beams dimensions	12 inch × 18 inch (305 mm × 457 mm)
Columns dimensions	12 inch × 12 inch (305 mm × 305 mm)
Concrete compressive strength, f_c.	4000 psi (28 MPa)
Yield strength of re-bars, f_y	60,000 psi (414 MPa)
Story-height	12 ft (3658 mm)
Total height	36 ft (11 m)—3-S, 48 ft (14.63 m)—4-S 60 ft (18.30 m)—5-S, 72 ft (22 m)—6-S

Table 5 Dynamic properties of as-built and retrofitted frames

Property	Value	
	As-Built	Retrofitted
Seismic floor weight	30.89 T	31.85 T
Total seismic weight of structure	93.45 T (3-S), 124.60 T (4-S) 155.75 T (5-S), 186.90 T (6-S)	96.33 T (3-S), 128.44 T (4-S) 160.55 T (5-S), 192.66 T (6-S)
Effective seismic weight of structure	74.37 T (3-S), 97.81 T (4-S) 125.10 T (5-S), 144.71 T (6-S)	76.74 T (3-S), 101.0 T (4-S) 125.35 T (5-S), 149.50 T (6-S)
Fundamental time period	0.84 s (3-S), 1.14 s (4-S) 1.56 s (5-S), 1.93 s (6-S)	0.67 s (3-S), 0.90 s (4-S) 1.11 s (5-S), 1.33 s (6-S)
Modal participation factor	1.25 (3-S), 1.26 (4-S) 1.27 (5-S), 1.28 (6-S)	1.25 (3-S), 1.26 (4-S) 1.27 (5-S), 1.28 (6-S)

Table 6 Seismic response parameters of ESB retrofitted RC frames. The values were rounded up

Model Col.: (1)	$T_{initial}$ (sec) (2)	F_{hinge} (kN) (3)	F_{max} (kN) (4)	Δ_y (mm) (5)	Δ_u (mm) (6)	μ (7)	R_μ (8)	Ω_0 (9)	R (10)
2-Story	0.46	142	265	71	168	2.37	2.37	1.86	4.41
3-Story	0.67	128	235	99	210	2.12	2.12	1.83	3.88
4-Story	0.90	119	227	131	285	2.18	2.18	1.90	4.14
5-Story	1.11	119	234	168	364	2.17	2.17	2.00	4.34
6-Story	1.33	112	229	200	432	2.16	2.16	2.05	4.43
Avg.							2.20	1.93	4.24

for eccentric braced frame. The floor level nodal displacements obtained for first mode was normalized such that the nodal displacement at roof level is 1.0. The normalized nodal displacements were used as a lateral displacement vector for displacement-control pushover analysis. The models were pushed laterally to a target roof displacement corresponding to roof drift of 2.0%, which was considered as a drift limit for the life safety performance level. The capacity curves were derived in the form of base shear and roof displacement for the considered ESB retrofitted frames. Figure 23 shows the capacity curves and their corresponding elasto-plastic idealization for computation of ductility
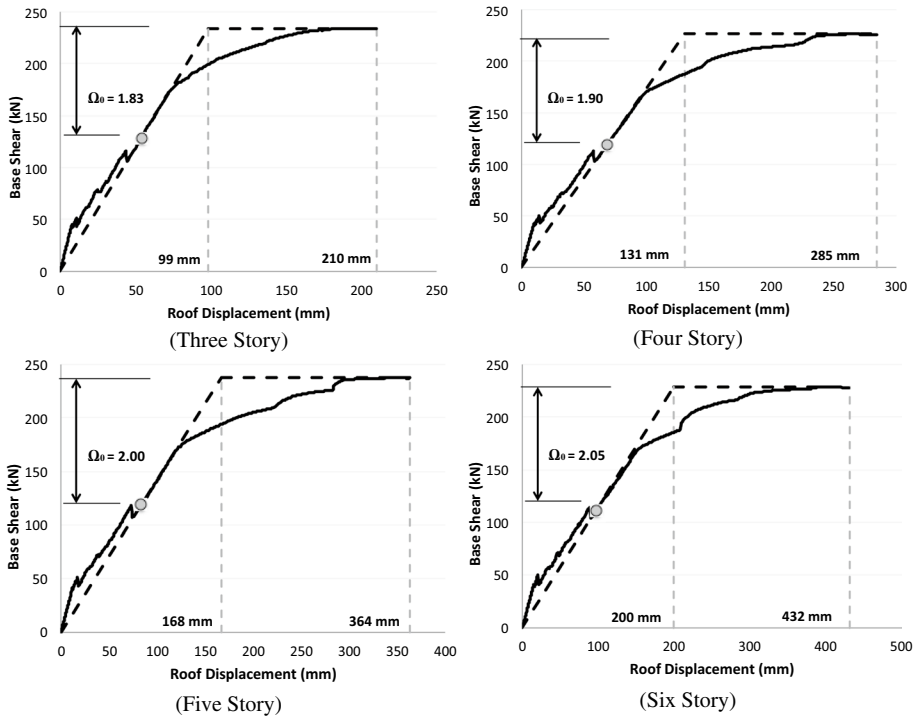
Fig. 23 Idealized elasto-plastic capacity curves for ESB retrofitted frames having 3, 4, 5 and 6 stories. Yield and ultimate displacements and overstrength factor for each frame are indicated on the plot

and overstrength factors. Each curve also indicates the formation of first flexure hinge in the beam.

Since, the lateral force corresponding to formation of first plastic hinge in beam was known, referred herein as F_{hinge} and reported in Col. (3) of Table 6, the corresponding displacement was identified on the capacity curve. These were used to calculate the initial stiffness of each frame. The idealized yield displacement was calculated dividing F_{max} (Col. 4, Table 6) by the initial stiffness, which is reported in Col. (5) of Table 6. Figure 23 also shows the derived idealized elasto-plastic capacity curves for ESB retrofitted RC frames.

The ductility factor R_μ of frames was calculated using the ductility-dependent response modification factor, as proposed by Newmark and Hall (1982):

$$R_\mu = 1 \quad T < 0.20 \text{ s} \quad \text{Short Period} \tag{16}$$

$$R_\mu = \sqrt{2\mu - 1} \quad 0.20 \text{ s} < T < 0.50 s \quad \text{Intermediate Period} \tag{17}$$

$$R_\mu = \mu \quad T > 0.50 \text{ s} \quad \text{Long Period} \tag{18}$$

where μ is the global structural ductility, which is the ratio of maximum displacement to the idealized yield displacement. The maximum displacement here corresponds to the life safety story-drift limit of ESB retrofitted RC frame. The maximum displacement and displacement ductility of each frame is reported in Col. (6) and Col. (7) of Table 6, respectively. T is the yield time period of idealized elastic–plastic representative SDOF systems of frames, which was found greater than 0.50 s for all structures. Therefore, R_μ of each frame was calculated using the relationship $R_\mu = \mu$, which is reported in Col. (8) of Table 6. The overstrength factor was calculated as the ratio of F_{max} to F_{hinge}, which is reported in Col. (9) of Table 6. The response modification factor of ESB retrofitted RC frame was calculated as, $R = F_E/F_y = F_E/F_y \times F_y/F_{hinge} = R_\mu \times \Omega_0$, which is reported in Col. (10) of Table 6. On average, response modification factor $R = 4.24$ (mean = 4.24 + Std. Dev. = 0.23), overstrength factor $\Omega_0 = 1.93$ (mean = 1.93 + Std.Dev. = 0.10) and ductility factor $R_\mu = 2.20$ (mean = 2.20 + Std.Dev. = 0.10) were obtained for ESB retrofitted RC frames.

5.3 NLTHA of ESB retrofitted multi-stories RC frames

The selected multi-stories ESB retrofitted RC frames were analyzed through nonlinear time history analysis (NLTHA) using the matched acceleration time histories for seismic performance assessment of frames under both the DBE and MCE ground motions. Figures 24, 25, 26 and 27 report peak inter-story drift demands on frames under acceleration time histories representative of both DBE and MCE ground motions, respectively. The maximum inter-story drift demands on structures under DBE and MCE ground motions, respectively, are as follows: 1.36% and 2.15% for three story frame, 1.57% and 2.29% for four story frame, 1.62% and 2.12% for five story frame, 1.63% and 2.11% for six story frame. The corresponding factor of safety are as follows: 1.56 and 1.36 for three story frame, 1.35 and 1.23 for four story frame, 1.30 and 1.27 for five story frame, 1.30 and 1.33 for six story
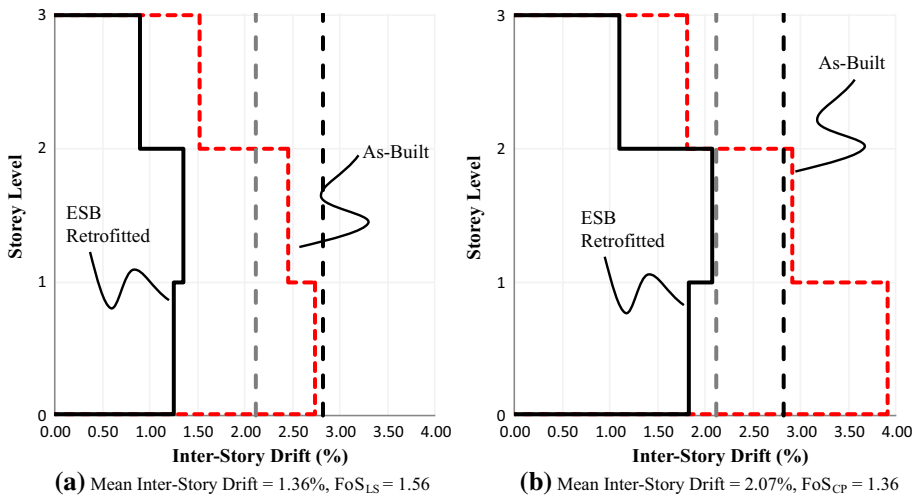

Fig. 24 Average inter-story drift demand on three-story frame under design base earthquakes (left) and maximum considered earthquakes (right). The story-drift capacity corresponding to LS (grey line) and CP (dark line) drift limits are also shown. Factor of safety (FoS) against the LS and CP levels are reported for ESB retrofitted frame

Fig. 25 Average inter-story drift demand on four-story frame under design base earthquakes (left) and maximum considered earthquakes (right). The story-drift capacity corresponding to LS (grey line) and CP (dark line) drift limits are also shown. Factor of safety (FoS) against the LS and CP levels are reported for ESB retrofitted frame
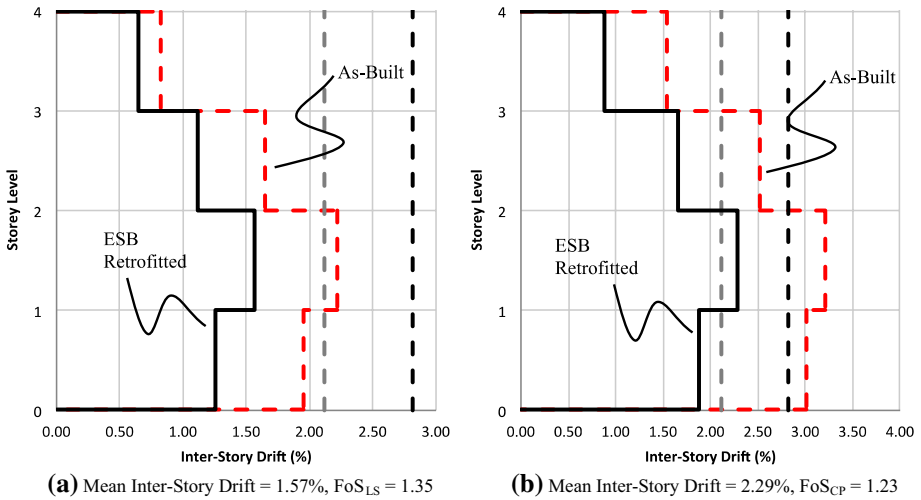

Fig. 26 Average inter-story drift demand on five-story frame under design base earthquakes (left) and maximum considered earthquakes (right). The story-drift capacity corresponding to LS (grey line) and CP (dark line) drift limits are also shown. Factor of safety (FoS) against the LS and CP levels are reported for ESB retrofitted frame
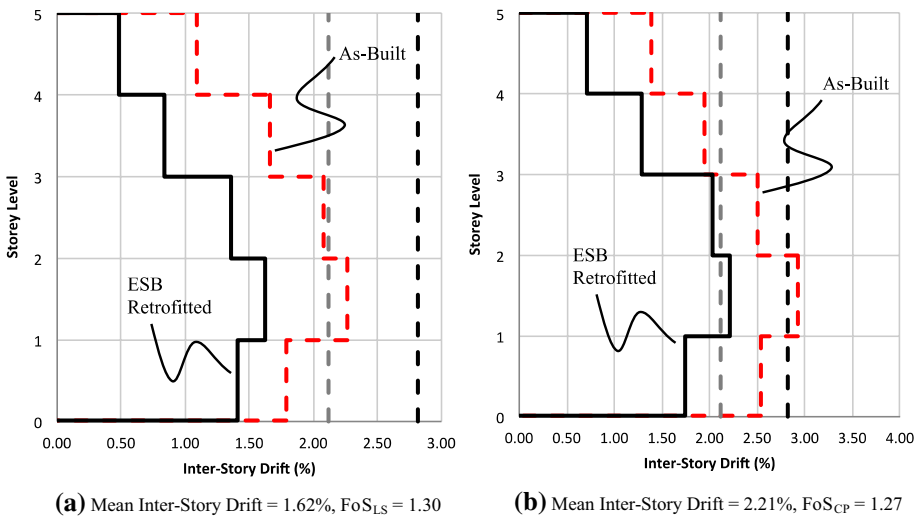
frame. This gives drift demand-to-capacity ratio as follows: 0.64 and 0.74 for three story frame, 0.74 and 0.81 for four story frame, 0.77 and 0.79 for five story frame, 0.77 and 0.75 for six story frame, exhibiting significant safety margin. Unlike the beam-sway mechanism of retrofitted frames, the counterpart as-built frames exhibited columns' yielding and
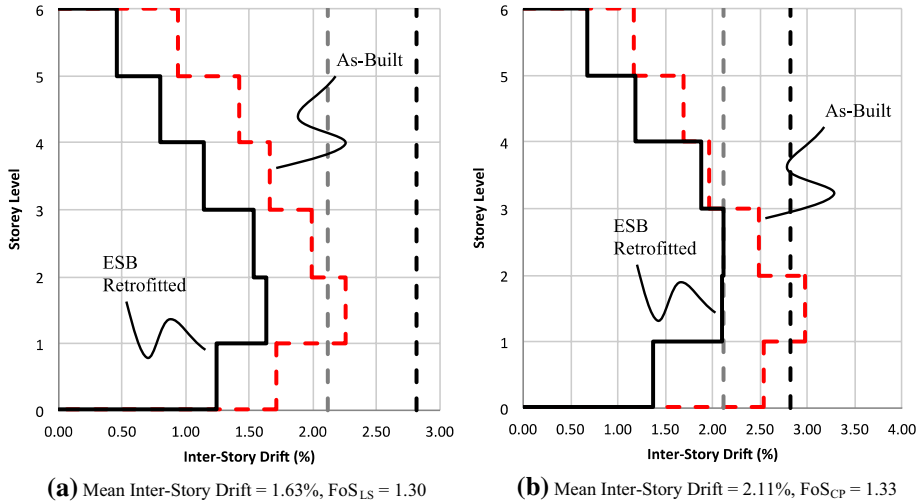
(a) Mean Inter-Story Drift = 1.63%, FoS$_{LS}$ = 1.30 **(b)** Mean Inter-Story Drift = 2.11%, FoS$_{CP}$ = 1.33

Fig. 27 Average inter-story drift demand on six-story frame under design base earthquakes (left) and maximum considered earthquakes (right). The story-drift capacity corresponding to LS (grey line) and CP (dark line) drift limits are also shown. Factor of safety (FoS) against the LS and CP levels are reported for ESB retrofitted frame

beam-column joints' shear hinging besides beams' yielding and exceeded the limit state drift capacities, indicating their seismic vulnerability and the beneficial role of ESB retrofit in controlling story-drift demand. The ESB retrofit has shown relatively better performance in case of low-rise structures in comparison to the high-rise structures. This is due to the fact that the same brace section was used in both low-rise and high-rise structures, to economize the retrofit scheme. A relatively stocky section may be used in case of mid-rise and high-rise structures to further improve the seismic performance of retrofitted structure.

It can be observed that seismic retrofit design of ESB frames with R = 3.50 can offer significant safety margin against both the DBE and MCE ground motions. This indicates that the ESB retrofit for the considered RC frame can be further economized by taking R = 4.0 in the seismic design of steel braces. It is interesting to mention that R = 4 was found reasonable also for eccentrically braced steel frame (Kuşyılmaz and Topkaya 2016). NLTHAs of multi-stories RC frames have revealed a non-uniform inelastic response of stories along the height with a trend to develop higher drift demand at middle stories, which is because an ESB retrofitted system responds almost similar to a dual system. However, as frame-like behavior is dominant the maximum inter-story drifts appear at middle stories.

6 Conclusions and recommendations

The following conclusions were made on the basis of experimental quasi-static cyclic tests performed on deficient and ESB retrofitted RC portal frames:

- The proposed ESB retrofitted scheme for deficient RC frame was capable to alter inelastic mechanism from column-mechanism and joint shear hinging to beam-mechanism with stable hysteretic response. This increased the hysteretic damping of deficient RC frame from 6 to 10%.

- The ESB retrofit increased the yield stiffness and yield strength of frame by 100% and 60%, respectively. However, only a marginal increase was noticed in the ductility of the frame.
- For retrofit design of RC frames with ESB, story drift of 2.0% and 2.50% can be reasonably considered as design and near collapse drift limits, respectively to provide appropriate safety margins.
- It was found that the simplified analytical drift model based on the rigid frame response underestimates the yield drift of ESB retrofitted frame by 75%. It is due to the fact that the basic equation ignores the contribution of shear deformation in link, flexure and shear deformation of beam outside the link, axial deformation of braces and columns, and deformation due to longitudinal re-bar slip/pullout in RC beams and columns. The present research recommends increasing the multiplying factor from 0.30 to 0.50 in the basic analytical drift model, in order to accurately predict yield drift of ESB retrofitted RC frame

$$\theta = 0.50 \left(\frac{\varepsilon_y}{h_b} \right) \left(\frac{L_1^2}{L_{bay}} \right) \tag{19}$$

  where ε_y is the yield strain of longitudinal rebar of beam, h_b is the depth of beam, L_1 is length of link beam and L_{bay} is the length of bay.
- The simplified analytical model of lateral strength, which is based on the global equilibrium consideration and plastic mechanism of frame, can be used in combination with the above drift model to develop capacity curve of ESB retrofitted RC frames. This can facilitate design and assessment of ESB retrofitted deficient RC frames.

The following conclusions were made on the basis of numerical study conducted on ESB retrofitted two-story RC frame:

- Comparison of numerical to experimental response of ESB retrofitted RC frame have revealed that nonlinear model prepared using inelastic force-based element with fiber-sections, and employing reinforced concrete models of Mander et al. and Manegetto-Pinto, can reasonably simulate force–displacement hysteretic response of frame in terms of maximum resistance, loading/unloading stiffness and in-cycle strength degradation. Most suitable parameters found for Manegetto-Pinto are: $R_0 = 19$, $b = 0.005$, $A_1 = 18.50$, $A_2 = 0.15$, $A_3 = 0.025$, $A_4 = 1$.
- Eccentric braces modeled with the in-built hollow structural section (HSS) given in SeismoStruct, and assigned with the fiber-section based force-based element, was found efficient in predicting the yielding mechanism of brace. Due to design consideration, and for simplification, the local/global buckling of braces were ignored in modeling.
- Nonlinear static pushover analysis of two-story ESB retrofitted RC frame exhibited significant hardening behavior. The first plastic hinge was formed in beam at a lateral load of 142 kN, however the structure achieved maximum lateral resistance of 256 kN. This gives structure overstrength factor $\Omega_0 = F_{max}/F_{plastic-hinge} = 256/142 \approx 1.86$. The capacity curve was bi-linearized in accordance with the FEMA P695 procedure, giving structure ductility capacity of 2.37 corresponding to story drift of 2.0%. This suggests $R_\mu = \mu = 2.37$. The total response modification factor $R = 4.41$ ($\Omega_0 \times R_\mu = 1.86 \times 2.37 \approx 4.41$) for the ESB retrofitted RC frame.

- The use of static force procedure of ASCE 7-16 and employing the AISC 360-16 building provisions for design of eccentric steel braces for seismic retrofitting of deficient RC frame, while considering response modification factor $R = 3.0_\mu$, will ensure formation of plastic hinges in beam and elastic response of steel braces. However, nonlinear static pushover analysis suggests even higher value may be taken even up to 4.41, which is about 47% higher than the initially assumed $R = 3.0$. This suggests, the seismic design of ESB retrofit can be further economized.
- NLTHA has revealed that the design base and maximum considered earthquakes were not able to push the frames beyond the LS and CP limit states, respectively. The ESB retrofitted RC frame possesses safety margins (drift capacity to drift demand ratio) of 1.63 and 1.56 against design base and maximum considered earthquakes, respectively. The satisfactory behavior is due to the fact that ESB retrofitting not only promotes a favorable plastic mechanism with stable hysteretic response but also increases the structure overstrength factor. The aforementioned large margins will also account for possible imperfections, which may be encountered in the field during execution of the retrofit scheme.

The following conclusions were made on the basis of numerical study conducted on ESB retrofitted multi-stories RC frames:

- ESB retrofitted multi-stories RC frames designed to $R = 3.50$, in which the RC components were designed for the 25% of lateral load, were analyzed through nonlinear pushover analysis giving seismic response parameters as $\Omega_0 = 2.20$, $R_\mu = 1.93$ and $R = 4.24$. It was observed that seismic retrofit design of ESB frames with $R = 3.50$ can offer significant safety margin against both the DBE and MCE ground motions. This indicates that the ESB retrofit for the considered RC frame can be further economized by taking $R = 4.0$ in the seismic design of steel braces. It is interesting to mention that $R = 4$ was found reasonable also for eccentrically braced steel frames (Kuşyılmaz and Topkaya 2016).
- NLTHAs have revealed a non-uniform inelastic response of stories along the height with a trend to develop higher drift demand at middle stories, which is because an ESB retrofitted system responds almost similar to a dual system. However, as frame-like behavior is dominant the maximum inter-story drifts appear at middle stories.

References

Abou-Elfath H, Ghobarah A (2000) Behaviour of reinforced concrete frames rehabilitated with concentric steel bracing. Can J Civ Eng 27:433–444

ACI-318 (2014) Building code requirements for structural concrete (ACI 318-14). American Concrete Institute, Farmington Hills

Ahmad N, Shahzad A, Ali Q, Rizwan M, Khan AN (2018) Seismic fragility functions for code compliant and non-compliant RC SMRF structures in Pakistan. Bull Earthq Eng 16(10):4675–4703

AISC 341-16 (2016) Seismic provisions for structural steel buildings. American Institute of Steel Constructions, Illinois

AISC 360-16 (2016) Specification for structural steel buildings. American Institute of Steel Construction, Illinois

ASCE 7-16 (2016) Minimum design loads for buildings and other structures ASCE/SEI 7-16. American Society of Civil Engineers

Badoux M, Jirsa JO (1990) Steel bracing of RC frames for seismic retrofitting. ASCE J Struct Eng 116(1):55–74

Basit A (2020) In-plane quasi static cyclic testing of frames strengthened with eccentric steel braces, Master Thesis, Department of Civil Engineering, UET Peshawar

Bush TD, Jones EA, Jirsa JO (1991) Behavior of RC frame strengthened using structural-steel bracing. ASCE J Struct Eng 117(4):1115–1126

Chaulagain H, Rodrigues H, Spacone E, Varum H (2015) Assessment of seismic strengthening solutions for existing low-rise RC buildings in Nepal. Earthq Struct 8(3):511–539

CSI (2014) SAP2000: integrated software for structural analysis and design. Computer and Structures Inc. (CSI), Walnut Creek

FEMA 356 (2000) Prestandard and commentary for the seismic rehabilitation of buildings. Federal Emergency Management Agency (FEMA), Washington, DC

FEMA 547 (2006) Techniques for the seismic rehabilitation of existing buildings. Federal Emergency Management Agency (FEMA), Washington, DC

Filippou FC, Popov EP, Bertero VV (1983) Effects of bond deterioration on hysteretic behaviour of reinforced concrete joints. Report EERC 83-19, Earthquake Engineering Research Center, University of California, Berkeley

Ghobarah A, Abou-Elfath H (2001) Rehabilitation of a reinforced concrete frames using eccentric steel bracing. Eng Struct 23:745–755

Higashi Y, Endo T, Shimizu Y (1981) Experimental studies on retrofitting of reinforced concrete structural members. In: Proceedings of the 2nd seminar on repair and retrofit of structures. National Science Foundation, Ann Arbor, MI, USA, pp 126–55

Hjelmstad KD, Popov EP (1984) Characteristics of eccentrically braced frames. ASCE J Struct Eng 110(2):340–353

Hjelmstad KD, Foutch DA, Del Valle E, Downs RE (1988) Forced vibration studies of an RC building retrofit with steel bracing. In: Proceedings of the 9th world conference on earthquake engineering, vol VII, pp 469–474

Khan MS (2020) Calibration and development of numerical model for inelastic seismic analysis of RC frame with weaker beam-column joint, Master Thesis, Department of Civil Engineering, UET Peshawar

Kim J, Choi H (2006) Displacement-based design of supplemental dampers for seismic retrofit of a framed structure. J Struct Eng 132(6):873–883

Kuşyılmaz A, Topkaya C (2016) Evaluation of seismic response factors for eccentrically braced frames using FEMA P695 methodology. Earthq Spectra 32(1):303–321

Lehman DE, Roeder CW, Herman D, Johnson S, Kotulka B (2008) Improved seismic performance of gusset plate connections. ASCE J Struct Eng 134(6):890–901

Lin YY, Tsai MH, Hwang JS, Chang KC (2003) Direct displacement-based design for building with passive energy dissipation systems. Eng Struct 25:25–37

MacRae GA, Kimura Y, Roeder C (2004) Effect of column stiffness on braced frame seismic behavior. ASCE J Struct Eng 130(3):381–391

Maheri MR, Sahebi A (1997) Use of steel bracing in reinforced concrete frames. Eng Struct 19(12):1018–1024

Mahrenholtz C, Lin PC, Wu AC, Tsai KC, Hwang SJ, Lin RY, Bhayusukma Y (2014) Retrofit of reinforced concrete frames with buckling-restrained braces. Earthq Eng Struct Dyn 44(1):59–78

Mander JB, Priestley MJN, Park R (1988) Theoretical stress-strain model for confined concrete. ASCE J Sturct Eng 114(8):1804–1826

Masri AC, Goel SC (1996) Seismic design and testing of an RC slab-column frame strengthened by steel bracing. Earthq Spectra 12(4):645–666

Mazza F (2019) A simplified retrofitting method based on seismic damage of a SDOF system equivalent to a damped braced building. Eng Struct 200:109712

Mazza F, Mazza M (2019) Seismic retrofitting of gravity-loads designed r.c. framed buildings combining CFRP and hysteretic damped braces. Bull Earthq Eng. https://doi.org/10.1007/s10518-019-00593-5

Mazza F, Vulcano A (2015) Displacement-based design procedure of damped braces for the seismic retrofitting of r.c. framed buildings. Bull Earthq Eng 13:2121–2143

Nakashima M, Wakabayashi M (1992) Analysis and design of steel braces and braced frames. In: Fukumoto Y, Lee GC (eds) Stability and ductility of steel structures under cyclic loading. CRC Press, Boca Raton, pp 309–322

Nateghi-Alahi F (1995) Seismic strengthening of eight-storey RC apartment building using steel braces. Eng Struct 17(6):455–461

Neuenhofer A, Filippou FC (1997) Evaluation of nonlinear frame finite-element models. ASCE J Struct Eng 123(7):958–966

Newmark NM, Hall WJ (1982) Earthquake spectra and design. Earthquake Engineering Research Institute (EERI), Oakland

Ohishi H, Takahashi M, Yamazaki Y (1988) A seismic strengthening design and practice of an existing reinforced concrete school building in Shizuoka city. In: Proceedings of the 9th world conference on earthquake engineering, vol VII, pp 415–420

Pinho R (2007) Nonlinear dynamic analysis of structures subjected to seismic actions. In: Pecker A (ed) Advanced earthquake engineering analysis. Springer, Berlin, pp 63–89

Popov EP, Engelhardt MD (1988) Seismic eccentrically braced frames. J Constr Steel Res 10:321–354

Priestley MJN, Calvi GM, Kowalsky MJN (2007) Displacement-based seismic design of structures. IUSS Press, Pavia

Rodrigues H, Varum H, Arêde A, Costa A (2012) A comparative analysis of energy dissipation and equivalent viscous damping of RC columns subjected to uniaxial and biaxial loading. Eng Struct 35:149–164

Roeder CW, Popov EP (1978) Eccentrically braced steel frames for earthquakes. ASCE J Struct Div 104(3):391–411

Roeder CW, Lumpkin EJ, Lehman DE (2011) A balanced deign procedure for special concentrically braced frame connections. J Constr Steel Res 67:1760–1772

Sen AD, Roeder CW, Lehman DE, Berman JW (2019) Nonlinear modeling of concentrically braced frames. J Constr Steel Res 157:103–120

Shibata M, Nakamura T, Yoshida N, Morino S, Nonaka T, Wakabayashi M (1973) Elastic-plastic behavior of steel braces under repeated axial loading. In: Proceedings of the 5th world conference on earthquake engineering, vol 1, Rome, Italy, pp 845–848

Sorace S, Terenzi G, Fadi F (2012) Shaking table and numerical seismic performance evaluation of a fluid viscous-dissipative bracing system. Earthq Spectra 28(4):1619–1642

Spacone E, Ciampi V, Filippou FC (1996) Mixed formulation of nonlinear beam finite element. Comput Struct 58(1):71–83

Sullivan TJ (2013) Direct displacement-based seismic design of steel eccentrically braced frame structures. Bull Earthq Eng 11(6):2197–2231

Tagawa Y, Aoki H, Huang T, Masuda H (1992) Experimental study of new seismic strengthening method for existing RC structure. In: Proceedings of the 10th world conference on earthquake engineering, pp 5193–5198

Tahamouli-Roudsari M, Entezari A, Hadidi MH, Gandomian O (2017) Experimental assessment of retrofitted RC frames with different steel braces. Structures 11:206–217

Tapia-Hernandez E, Garcia-Carrera S (2019) Inelastic response of ductile eccentrically braced frames. J Build Eng. https://doi.org/10.1016/j.jobe.2019.100903

Tremblay R, Timler P, Bruneau M, Filiatrault A (1995) Performance of steel structures during the January 17, 1994, Northridge earthquake. Can J Civ Eng 22(2):338–360

Tremblay R, Bruneau M, Nakashima M, Prion HGL, Filiatrault M, DeVall R (1996) Seismic design of steel buildings: lessons from the 1995 Hyogoken Nanbu earthquake. Can J Civ Eng 23(3):757–770

Usami H, Azuchi T, Kamiya Y, Ban H (1988) Seismic strengthening of existing reinforced concrete buildings in Shizuoka prefecture, Japan. In: Proceedings of the 9th world conference on earthquake engineering, vol VII, pp 421–426